AD-A159 460 PLASMAS AS LIGHT SOURCES FOR LASERS(U) ALABAMA UNIV IN HUNTSVILLE T A BARR ET AL. SEP 84 AMSMI/RH-CR-85-14 1/1
DAAH01-82-D-A016

UNCLASSIFIED F/G 20/5 NL

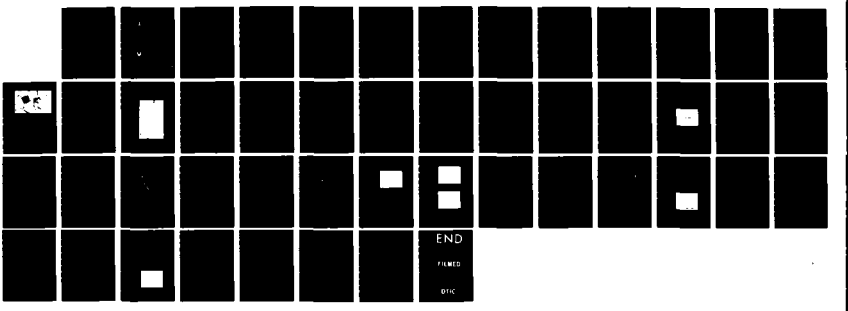

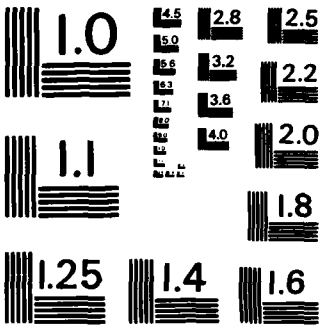

MICROCOPY RESOLUTION TEST CHART
NATIONAL BUREAU OF STANDARDS-1963-A

(2)

AD-A159 460

TECHNICAL REPORT RH-CR-85-14

PLASMAS AS LIGHT SOURCES FOR LASERS

T. A. Barr, Jr.
W. B. McKnight
The University of Alabama in Huntsville

for:

Directed Energy Directorate
Research, Development, and Engineering Center

SEPTEMBER 1984

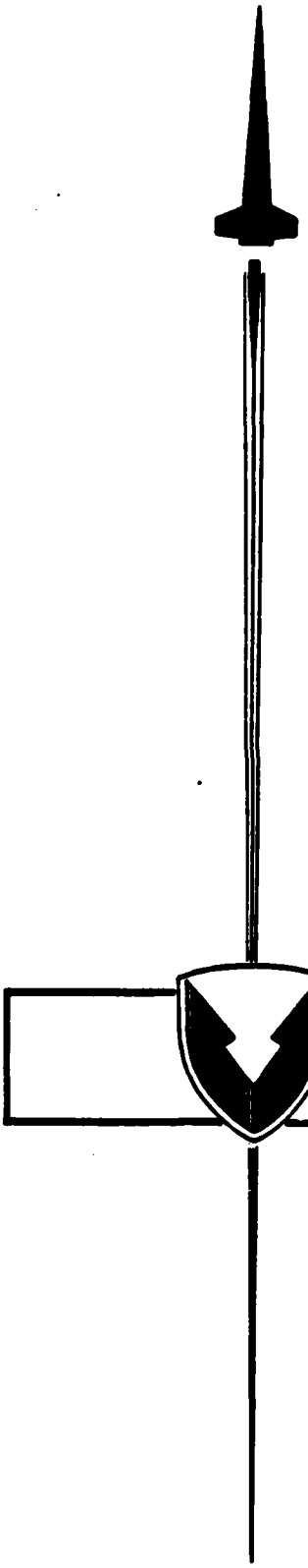

U.S. ARMY MISSILE COMMAND
Redstone Arsenal, Alabama 35898-5000

Cleared for public release; distribution unlimited.

DTIC FILE COPY

DTIC
ELECTE
OCT 1 1985
S D
B

SMI FORM 1021, 1 AUG 85 PREVIOUS EDITION IS OBSOLETE

85 09 30 060

DISPOSITION INSTRUCTIONS

WHEN THIS REPORT IS NO LONGER NEEDED, DEPARTMENT OF THE ARMY ORGANIZATIONS WILL DESTROY IT IN ACCORDANCE WITH THE PROCEDURES GIVEN IN AR 380-5.

DISCLAIMER

THE FINDINGS IN THIS REPORT ARE NOT TO BE CONSTRUED AS AN OFFICIAL DEPARTMENT OF THE ARMY POSITION UNLESS SO DESIGNATED BY OTHER AUTHORIZED DOCUMENTS.

TRADE NAMES

USE OF TRADE NAMES OR MANUFACTURERS IN THIS REPORT DOES NOT CONSTITUTE AN OFFICIAL INDORSEMENT OR APPROVAL OF THE USE OF SUCH COMMERCIAL HARDWARE OR SOFTWARE.

UNCLASSIFIED

SECURITY CLASSIFICATION OF THIS PAGE (When Data Entered)

REPORT DOCUMENTATION PAGE		READ INSTRUCTIONS BEFORE COMPLETING FORM
1. REPORT NUMBER TR-RH-CR-85-14	2. GOVT ACCESSION NO. AD-A159460	3. RECIPIENT'S CATALOG NUMBER
4. TITLE (and Subtitle) Plasmas as Light Sources for Lasers		5. TYPE OF REPORT & PERIOD COVERED Technical Report 6. PERFORMING ORG. REPORT NUMBER
7. AUTHOR(s) T. A. Barr, Jr. W. B. McKnight		8. CONTRACT OR GRANT NUMBER(s) Final Report BMD Contract DAAH01-82D-A016
9. PERFORMING ORGANIZATION NAME AND ADDRESS The University of Alabama in Huntsville Huntsville, Alabama 35899		10. PROGRAM ELEMENT, PROJECT, TASK AREA & WORK UNIT NUMBERS
11. CONTROLLING OFFICE NAME AND ADDRESS Commander, US Army Missile Command ATTN: AMSMI-RH Redstone Arsenal, AL 35898-5245		12. REPORT DATE September 1984 13. NUMBER OF PAGES
14. MONITORING AGENCY NAME & ADDRESS(if different from Controlling Office)		15. SECURITY CLASS. (of this report) UNCLASSIFIED 15a. DECLASSIFICATION/DOWNGRADING SCHEDULE

16. DISTRIBUTION STATEMENT (of this Report)

Cleared for public release; distribution unlimited.

17. DISTRIBUTION STATEMENT (of the abstract entered in Block 20, if different from Report)

18. SUPPLEMENTARY NOTES

19. KEY WORDS (Continue on reverse side if necessary and identify by block number)

Lasers
Plasma
Pulsed discharges

20. ABSTRACT (Continue on reverse side if necessary and identify by block number)

This report describes an experimental and analytical investigation of the properties of high intensity, visible wavelength, light sources for optical pumping of pulsed lasers. Background information on research that may be applicable to this problem is presented, the experiment design is outlined and the results of system modelling are detailed. The experimental apparatus, consisting of a Blumlein pulse-forming network and a cylindrical plasma cell

(Continued)

DD FORM 1 JAN 73 1473 EDITION OF 1 NOV 65 IS OBSOLETE

SECURITY CLASSIFICATION OF THIS PAGE (When Data Entered)

20. (Continued)

load, is described. The instrumentation used for the experiment is discussed, and experimental results are presented, together with a possible explanation of the optical radiation-time history of the plasma. Potential applications are evaluated and future development recommended.

TR-RH-CR-85-14 September 1984

PLASMAS AS LIGHT SOURCES FOR LASERS

Final Report
BDM Contract DAAH01-82D-A016
Task Order No. 0001

Prepared by:
T. A. Barr, Jr.
W. B. McKnight
The University of Alabama in Huntsville

Directed Energy Directorate
Research, Development, and Engineering Center
US Army Missile Command
Redstone Arsenal, AL 35898

CONTENTS

I. TASK ORDER CRITIQUE

The technical requirements for this task as shown in the Statement of Work are listed below and are numbered as they appear in the task order.

2.1 The subcontractor shall construct or obtain the remaining components needed to assemble the planned experiment.

2.2 The subcontractor shall supply all components generated under requirement 2.1, above, to the Government for installation in building 8971 or other site at the option of the Government. The Government will, in its own facilities, provide all other items and services required to complete and conduct the experiments.

2.3 The subcontractor shall monitor the installation and operation of the experimental apparatus and the Government execution of the experiments. These experiments shall include but not be limited to the measurement of energy input, development, and characteristics of the plasma and/or laser.

2.4 Results of the experiments shall be analyzed and a final report prepared by the contractor. This report shall also include:

2.4.1 A description of the experimental equipment, both that supplied by the contractor and that supplied by the Government.

2.4.2 A critique of the potential applications of the investigated light source and lasers, and

2.4.3 Recommendations for future development of light sources of lasers of the type investigated under this contract.

II. RESPONSE TO THE SOW TECHNICAL REQUIREMENTS

2.1 The planned experiment called for the construction of a capacitor bank as the power source for the plasma discharge cell which is GFE and the procurement of instrumentation to measure radiation integrated energy, pulse shape, spectral composition, and other properties such as the voltage and current in the discharge. Under this task order, we have assembled twelve capacitors as a Blumlein network and attached this line to the plasma discharge cell. Further, we have assembled and tested the instrumentation for the experiments.

2.2 The equipment above has been tested and is available to the Government as stated under the provisions of this part of the task order. However, the Government's technical representative has requested that the experiments be conducted at the University of Alabama in Huntsville and we have agreed to do that. Experiments have already been started.

2.3 The experiments are being conducted at the contractor's facilities and by contractor personnel, so the contractor monitoring function is taken care of automatically. The measurement of input and output parameters was accomplished as specified.

2.4 The results of the experiments have been analyzed and are included in this report. Also included, as required, are the descriptions of all the equipment peculiar to the experiment, a critique of the potential applications of the light source and laser, and recommendations for future development of light sources for lasers of the type investigated under this task order.

This report describes the work done, both computationally and experimentally, to accomplish the objectives of the task order. Following the design criteria set up in the previous work (re: Subcontract No. BDM-D-376-00MAAA, Task No. 0001), we purchased 15 0.7 microfarad, 50 kV capacitors having reverse voltage tolerance of 40 kV. Twelve of these capacitors have been incorporated into a Blumlein network to serve as a pulsed power source for the discharge which produces the plasma light source. Under the present task order, we have constructed, tested and used this power source to produce the plasma light source for laser pumping. The capacitor bank will hold, at 50 kV, 10,500 joules of electrical energy. If reasonable impedance matching can be maintained, approximately 80 percent to 90 percent of the energy can be transferred to the plasma in about 10 microseconds. Experiments are underway to determine the actual energy transfer to the plasma and the eventual transfer of radiation in a useful band to a laser rod or dye solution. We have already demonstrated the radiation output pulse shape and duration for a range of pressures in argon.

III. BACKGROUND INFORMATION

In the first task period the pertinent literature on plasma light sources was reviewed and a comprehensive review made based on reference citations in "Physics Abstracts, A" dating from ca, 1973 to the present. Secondary citations carried the search back to 1960. Over forty papers were selected for detailed study. These covered:

(a) Ten papers on Mather type discharges

(b) Three papers on hypocycloidal discharges

(c) Four papers on imploding gas "shells"

(d) Two papers on imploding wire arrays

(e) Two papers on imploding metal shells

(f) Three papers on Z and θ pinches

(g) Five papers on exploding wires

(h) Six papers on spark discharges

(i) Two papers on surface sparks

(j) Eight papers on numerical analyses, primarily on fluid and plasma dynamics of implosions

(k) One paper on expanding plasma in a gas, and

(l) Four papers on instruments and controls relating to the above phenomena.

The primary thrust of the works reported in these papers was the attempt to produce plasmas suitable for controlled thermonuclear reactions in deuterium gas (or similar things); thus, the most "successful" workers reported x-ray production from plasmas in the 1-2 keV range. Two articles, however, had technology which we consider to be transferable to our needs [1,2]. Even here, the plasma energy was about 12 eV where our requirements are for 2-4 eV.

The work of Turchi and Baker [1] on the generation of high energy plasmas by electromagnetic implosion contains what appears to be all essential ingredients for our proposed plasma light source experiments. Their goal was to show how to obtain a multimegajoule high-temperature plasma. They were specifically trying to efficiently couple large quantities of energy from a capacitor bank to a cylindrical plasma. Direct ohmic heating of the plasma was rejected as a technique since the plasma radiative dissipation rate increases rapidly with temperature [$(0)T^4$] so there is a marked drop in efficiency of heating as the temperature gets close to 50 eV even for megampere currents. Our requirements, as relatable to the pumping of either glass or dye lasers, are for peak output in the visible (or near uv) spectrum around 2 to 4 eV. Also we must determine the optimum time for the plasma to pump the laser, which may be long, i.e., 1-10 μs. With the lower peak temperature requirement and the possibly longer plasma radiation time requirement, the pumping of energy into the plasma by the means described by Turchi may be neither desirable nor effective. Their radiation goal was $\sim 10^{14}$ W in 1 + μ sec.

The advantage of the transfer of energy to the plasma by $\underline{j} \times \underline{B}$ forces instead of direct ohmic heating is that energy may be added, almost without loss, as kinetic energy of motion instead of as heat. Heating occurs during the 10 to 50 n sec that the imploding gas has stopped its inward motion. There the kinetic energy is converted to thermal energy and is quickly radiated as a light pulse.

Turchi and Baker [1] have calculated that neither viscosity (viscous Reynolds number, $R_{ey} \sim 10^6$) nor magnetic forces (magnetic Reynolds number, $R_m \sim$ 100-300) are major factors in the plasma motion. And since $R_{ey} >> R_m$, there are no appreciable viscous effects in the boundary layer either.

The dominant hydrodynamic instability is considered to be the Rayleigh-Taylor (R-T) instability (ies). Successful passage through the R-T domain is:

$$[\tau_{R-T}] \frac{d}{dt}\left(\frac{B^2}{2\mu}\right) >> P \qquad (1)$$

where τ_{R-T} is the characteristic growth time for R-T instabilities, $B^2/2\mu$ is the magnetic pressure, and P is the plasma pressure. The R-T criterion is most suited to the current sheath around a cylindrical plasma core. In our experiments the plasma itself is in a thin, rapidly moving cylindrical sheet. In a later work by Baker, et al [3], an experimental measurement of instability in an imploding metal sheath showed a possible kink instability under high current, thick (nonvaporized) foil pinching. This does not appear to happen for thin foils and we thereby presume it does not happen for plasma sheaths, at least in the area of our interests.

In order to overcome nonuniform initiation, we will also study the variations on discharge techniques as described by Roberts [4] in which multiple wires were used as input conductors and by Degnan and Reinovsky [2], by Benjamin, et al [5], and by Gersten, et al [6], in which either multiple wires or multiple gas jets took the place of the evaporating foil liner.

A first-order theory to model an imploding plasma with particular attention being given to MHD instabilities has been described in a paper by Hussey, et al [7], for the exact cases experimentally examined by Turchi and Baker [1], and Baker, et al [3]. We will attempt to use this work, scaled down to our requirements, to model our experiments on imploding plasmas.

In general, we were disappointed in the lack of transferable technology to meet our requirements. Several authors reported successful attempts to use the Mather discharge and hypocycloidal discharge to pump dye, xenon recombination and iodine dissociation lasers. Most were done as "after thoughts" on devices designed for high energy plasma experiments. Lee, et al., (1980)[8] were able to convert a hypocycloidal device, which at first made hot plasma, Te $\sim$ 1 keV and 10^{19} /cc ions, into a cold plasma device at T_e = 1 eV and 10^{18} /cc ions. Incidentally this experiment showed why there may be a need for a plasma light source - especially for lasers with fast decay processes. They report that the UV intensity from their hypocycloidal device was 150 times as strong as that from a standard flash lamp which has comparable dimensions and a pulse duration 100 times longer than the hypocycloidal discharge. Lee [8] makes a very persuasive case for the hypocycloidal discharge as an optical pump for lasers. In a later work, Fanning and Kim (1983)[9] demonstrate the pumping of a dye laser by a Mather type discharge and state their preference for this type over the hypocycloid discharge because they believe that the laser tube may block part of the hypocycloidal discharge. This, however, may not be a problem since a high pressure (26.6 kPa) argon hypocycloidal discharge has a hollow core. One should note that Kozlov and Protasov (1976) were probably the first to report the pumping of a dye laser with a Mather type discharge (or similar discharge).

No one appears to have attempted to pump a laser with a coaxial electrically-produced plasma using a linear (Z type) discharge. Most Z discharge work has been directed towards producing the highest possible plasma energy with radiation in the keV range. Such radiation is completely wasted on the visible wavelength lasers which require visible and near UV photon pumping. It is our intent to investigate the cylindrical plasma produced from a thin metal film, plated on the inside of a glass tube, by an intense electric discharge. By proper control of the system geometry, film type, thickness and discharge characteristics, we expect to produce plasmas

which radiate in the 2-5 eV range where the optimum optical pumping for dye and Nd lasers occurs. Such a plasma can be controlled in density and in temperature, and further it may, through the $\underline{j} \times \underline{B}$ forces, be forced to collapse on the sidewall surface of a cylindrical laser. This latter property should greatly enhance the radiation coupling between the plasma and the laser.

IV. EXPERIMENT DESIGN

A. Rationale

The ultimate objective of this work is the production of a powerful pulsed visible-wavelength laser. The plasma light source has the potential for optically pumping a laser in a few microseconds with a correspondingly short, high power output. This is not a "Q" switch but rather a so-called "gain-switched" pulse. The inversion is built up to a high level in both cases - here it is done by intense, rapid pumping, rather than by keeping the cavity "Q" at a very low value.

Items which must be considered in the design of the system are:

1. Type of laser(s) suitable for rapid pumping,
2. Pump intensity and wavelength band for optimum pumping,
3. Tolerance of the laser to out-of-band radiation generated in the pump plasma or means for reducing out-of-band radiation on the laser,
4. Plasma generation for the desired radiation band: this includes the questions of type of parent material for the plasma, and
5. Electrical and geometrical configurations to meet the system requirements.

These questions were addressed in the original task and results were reported there. Based on our answers, we proceeded to design a plasma generator and its power supply. We also developed several computation routines which aided in the design of the combined plasma generator and power supply system. A Transient Circuit Analysis (TCA) program was used along with the routines for determining capacitance and inductance of wire and gas conductor arrays to produce a computational model which could be used as a design aide for construction of the system.

The design for the experiments involved (1) the selection of the type of lasers to be pumped optically with plasma radiations, (2) the selection of the plasma generator, and (3) the selection of the power source. The laser(s) to be tested are those chosen during the first phase of this work, namely, a Nd:glass laser, a dye laser, and a metal vapor plasma laser. While the full range of laser types cannot be tested under the present task, they have been considered in the overall design of the experiment equipment. In selection of the plasma discharge configuration, the size and shape of the Nd:glass rod was considered, along with the possibility of eventually using the system for a dye laser. This placed a very small, lower limit on the system size,

since Nd:glass lasers are only a fraction of a centimeter in diameter and a few centimeters long can work well. Even lower limits on sizes can be argued for dye lasers. In our case, however, we want to consider scaling to high power and so have chosen to make the system as large as we can in a practical sense. The system size was, therefore, governed more by funding and time limitations than by minimum or maximum laser size. Our selection of a 10 kilojoule capacitor bank was also based on the plausibility for scaling up from our configurations. The users' applications will probably require ten to fifty fold increase in size from our experiments, and consequently, our work will be a basis for scaling.

B. Design of the Plasma Generator Cell (Plasma Light Source)

In designing a plasma light source which is a Z pinch, coaxial with the laser, a number of physical conditions and effects must be considered:

1. Is the plasma opaque, translucent or transparent?

2. Is energy moving into and out of the plasma efficiently; i.e., are power source and plasma impedance matched, and is the radiation being emitted in the right band with the right intensity and duration?

3. Is the plasma radiation efficiently coupled into the laser?

Our design goal is to produce plasma which has a characteristic temperature in the 2-5 eV band. From past work, e.g., Lee, et all (1980 [8] and our own work, plasma ion/election density for this temperature will probably in the 10^{19} /cc - 10^{18} /cc range. Such a plasma in an electric discharge should provide major radiation stimulation for the non-ionized residual metal vapor. The design for the plasma light source is based on the simplest possible working concepts. We have as our first principle chosen to balance energy input-output requirements. We have attempted to provide matched source-plasma electrical impedance over physically plausible ranges of power, impedance, voltage, time, etc. We have designed-in certain configuration flexibility which permits us to change electrical source impedance/power/voltage, etc., over wide ranges. We have provided for alternative optical configurations which permit diagnostics of the plasma, insertions of a laser rod, eg Nd:glass, or the application of laser optics directly to the plasma.

The design of the plasma generator cell follows the technique of Roberts [4] in his use of a multiple conductor return path for a coaxial discharge. The plasma cell (GFE) also permits the inclusion of auxiliary "shells" in which filter material and/or fluorescent material may be placed to alter the radiation band reaching the laser. With minor modification, the same apparatus can be made into a plasma laser, thus providing a versatile basic piece of equipment to perform a series of experiments on plasmas as radiation pumps for driving lasers.

Figure 1 is a photograph of the plasma generator cell. The insert sketch shows the cross section of the cell at the indicated location (Section a-a). The plasma cell consists of three concentric glass tubes surrounded by an array of eight conductors. The length of the discharge

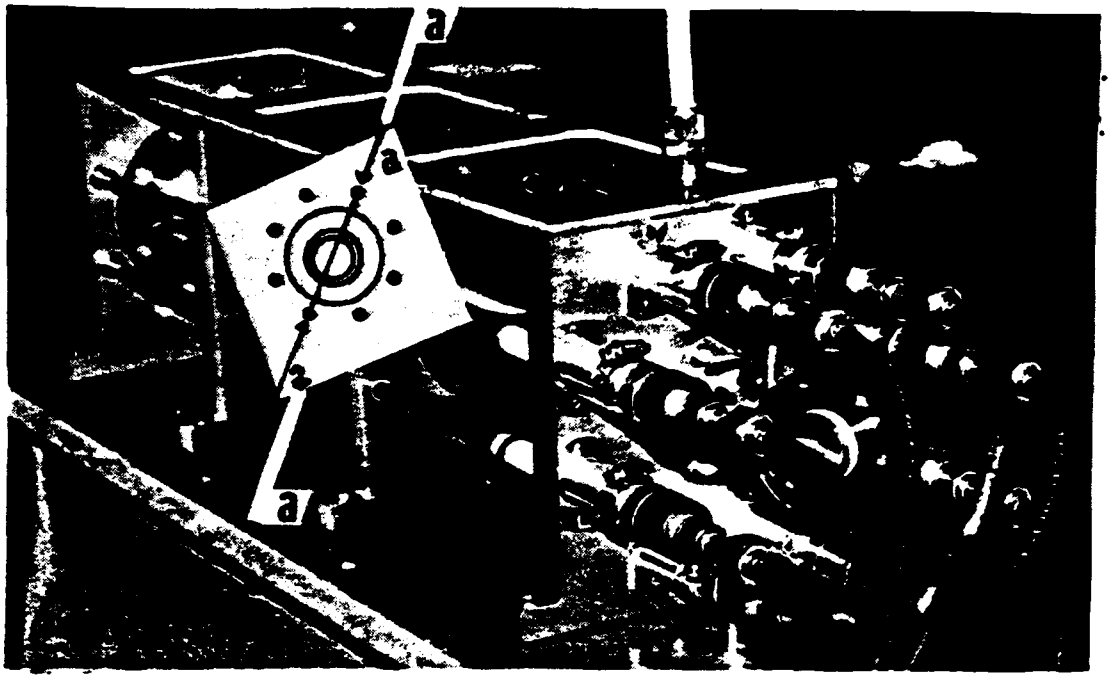

Figure 1. Plasma generator cell.

path, which is in the gap between the outer and first inner glass tubes, is about 60 cm. The outer glass tube, made of "Pyrex" glass, is 10 cm diameter, and the first inner tube, made of fused silica, is 3.8 cm. The second inner tube, also of fused silica, has an outer diameter of 2.5 and an inner diameter of 2.2 cm. The eight return conductors are equally spaced around a circle 15 cm in diameter and are each .95 cm diameter.

C. Design of the Power Supply

A number of electrical pulse forming networks were considered for the plasma light source. The one which was selected is the Blumlein network. A comparison of various possible sources shows why the Blumlein network was chosen. The following power supplies were considered:

1. Thyratron pulse transformer: This is a standard combination for producing long trains of pulses. The thyratron and transformer technologies are mature and their upper limits of voltage are well above the 50 kV which we believe to be sufficient. The waveform has an inherent "droop" which is generally considered to be a disadvantage but in our case, would be an advantage in limiting the current and holding the gas impedance up during the discharge. This system does have the disadvantage of active electronics, requiring considerable expense ane construction costs in getting a system together, tested and put into the laboratory. Also, the upper current limit for commercial thyratrons is about 20 kAmps., which is about half of the amperage we will eventually need.

2. Marx bank: This standard, passive network power source is still a possible choice for some work requiring a rapid voltage rise and a very high voltage on the load (as would be the case for high pressure gas discharges). The low voltage per stage is a distinct advantage, but the multiple, simultaneous switching is difficult to time and certainly is a problem in repetitively pulsed systems. In our case, where single discharge of the power supply is the mode of operation, the multiple switches can be left to run in rapid succession and the events can be timed from them instead of the outer way around. Marx banks also appear to have no scaling limits.

3. The simple type "E" transmission line can also be used as an energy storage and transfer system. This line has a rapid rise in voltage and in general produces a single square pulse when properly impedance matched. It has the disadvantage of requiring a transfer switch and the resultant voltage pulse is one half the charge voltage.

4. The Blumlein network is the system of choice for our application. The waveform, generally perceived as a disadvantage, is a single, almost-triangular pulse. The network switch is remote from the "work" or "load", and the gradual rise is an advantage in our case, especially where the electrical heating and evaporation of a metal film on the inside of the discharge tube is to be used. This network, when loaded at its characteristic impedance, produces full charging voltage on the load.

5. Darlington networks: The Blumlein is a special case of this kind of network and other Darlington networks can produce higher voltages when properly constructed. However, they are generally "point design" networks and we need as general a power supply as can be tolerated by the load, due to our changing experimental conditions. In many cases this network cannot be used because of its inherent slow voltage rise time.

Our selection of the Blumlein network is based on the perceived need for no voltage on the plasma tube until the exact firing time, the possible need for a double source voltage to initiate breakdown of the gas in the plasma cell, and the plasma cell's tolerance of a rather slow rise time for the current (ca. 1-2 microseconds). The configuration of this network provides for an easy change to the type E line but would require some re-engineering to produce a lumped capacitance configuration such as a Marx bank or the circular configuration as used in some thermonuclear experiments. Figure 2 is a photograph of the Blumlein network which was built for this research. The twelve capacitor Blumlein network is the power supply for the plasma generator cell. The plasma cell, out of the photo to the right, is connected to the cases of each row of condensors. The spark gap at the lower left "inverts" the front row of capacitors thereby placing a voltage on the plasma generator cell. The coil at upper left is a conduction path to restore the potentials of the front row of capacitors to ground after the discharge occurs.

V. SYSTEM MODELLING

A. Calculations of Plasma Cell Characteristics

The general power requirement and the GFE plasma cell were the starting points for the design. As discussed in our report on task 0001, we

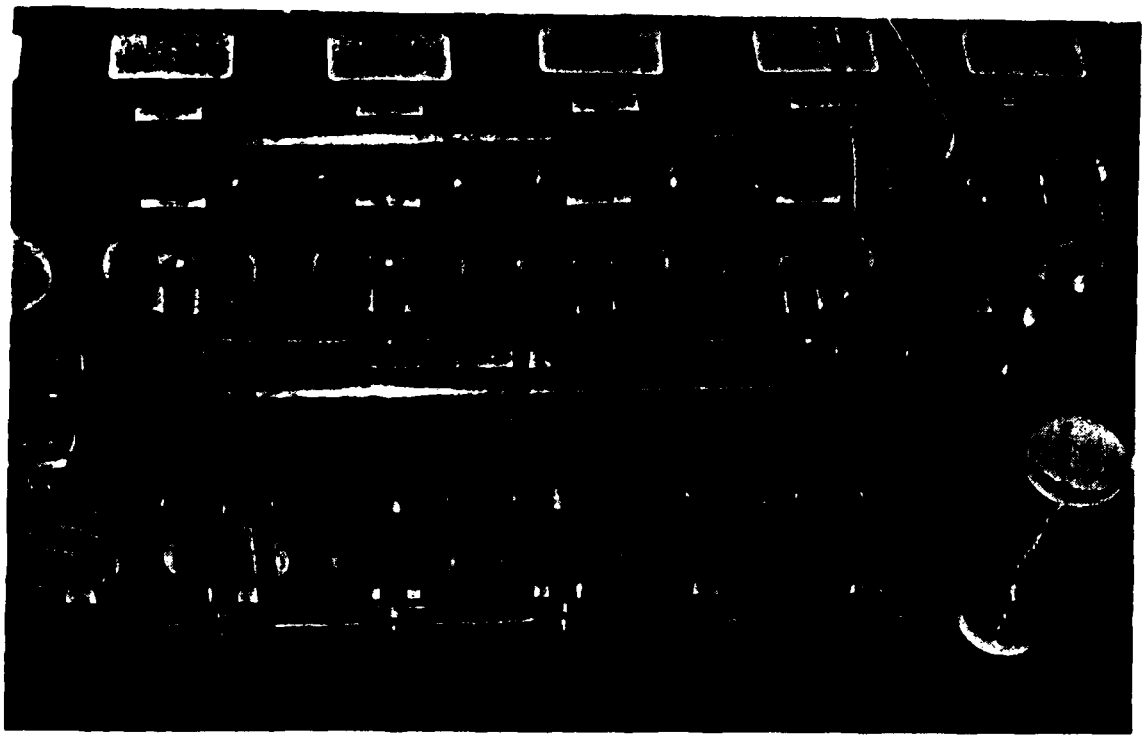

Figure 2. Blumlein network.

plan to eventually generate a plasma from an evaporated metal film which will initially exist as a coating on the inside of the plasma discharge tube. Then, after evaporation by the electric current, the metal vapor will be electrically heated to the plasma state. The properties of the initial film and the energy budget for its conversion to a radiating plasma were described in the previous report. Work in this task was directed towards detailed design assembly and testing of the system.

A primary consideration was the electrical characterization of the plasma discharge tube. In order to calculate the impedance of this tube we must consider the capacitance and inductance of the tube when the discharge is under way. This means that a varying diameter must be assigned to the plasma column as it progresses from the inside of the outer tube to the outside of the intermediate tube. Both the inductance and the capacitance of the plasma discharge tube will change during the discharge as a result of this. The changing induction and capacitance along with the discharge resistance, will create a changing load impedance. Our basic formulae for this type coaxial system were obtained from Gilder (Reference 10) and Grover (Reference 11) and the National Bureau of Standards (Reference 12) and were incorporated into our computer routines.

The calculation of the resistance of the plasma discharge "ab initio" is beyond the scope of our effort. However, with the use of data obtained from similar discharges, we can estimate the resistive component of the total reactance of the discharge. This, along with the calculated inductance and capacitance, will give a reasonable value for the total impedance of the plasma discharge. We used the data from References 13 and 14 as the basis for estimating the free electron density and mobility in the plasma and assumed that we would meet our goal of having a 2 eV plasma.

The plasma cell was modelled using formulae from References 10, 11, and 12. We obtained both the inductance and capacitance and thus the characteristic impedance of the plasma cell. A refinement of the program using these formulae made it possible to calculate the changing impedance of the discharge as the plasma pinched during the discharge. The inductance, capacitance and resultant impedance of the plasma and return conductors are shown in Table 1. Figure 3 shows the variation of the cell impedance as a function of plasma diameter. The part of the impedance due to reactive components increases with time due to the collapse of the central current conductor, as would be the case for a plasma pinch discharge. We also know from previous experience that the resistive component of reactance drops markedly due to the kinetics of discharge initiation in a gas.

The inductance, capacitance and reactive impedance of the plasma generator cell which is an array of parallel wires on the surface of a right circular cylinder with a hollow return conductor in the center which has the following properties: wire diameter is .95 cm.; there are 8 wires; the cylinder radius is 7.5 cm.; the center conductor's outer diameter is 10 cm and its thickness is .5 cm; the length of the array is 60 cm.

TABLE 1. Inductance Capacitance and Reactive Impedance of the Plasma Generator Cell.

CORE RAD.	INDUC.	CAPACIT.	IMPED.
cm	μ hys	μ fds.	ohms.
2.5	.153	7.13E-05	46.32
2.4	.159	7.03E-05	47.53
2.3	.164	6.94E-05	48.61
2.2	.17	6.84E-05	49.83
2.1	.176	6.75E-05	51.06
2	.182	6.65E-05	52.29
1.9	.189	6.55E-05	53.68
1.8	.196	6.46E-05	55.07
1.7	.203	6.36E-05	56.48
1.6	.211	6.26E-05	58.04

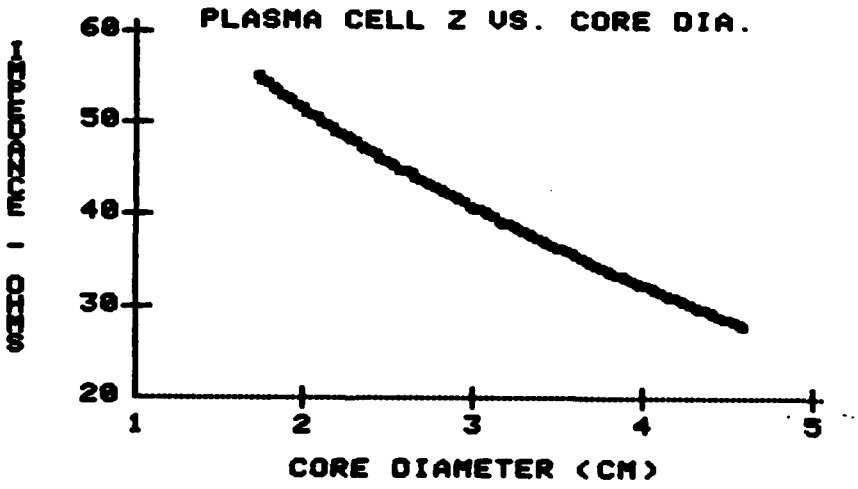

Figure 3. Calculated impedance of plasma cell as the core collapses (z pinch) from inside of outer wall to outside of intermediate wall. (See Table 1).

B. Power Supply Modelling

The next consideration was the modelling of the power supply network. The large capacitance required for the energy storage means that the inter-connecting inductances must be small to produce the discharge in the desired time. For example, if each of the twelve capacitors is considered as an independent element in a lumped transmission line, then the time constant for that capacitor and its associated inductance should be 1/12 of 10 microseconds, or 0.85 microseconds. The internal inductance of each capacitor is 40 nanohenries and, since the total inductance in microhenries for the element is $H(tot.)=(0.85)^2/F$ where F is the capacitance in microfarads, then the external inductance is 0.99 microhenries. From our table of straight wire inductances, we find that 103 cm of straight tubing, 1.6 cm diameter (5/8"), will produce the desired inductance. The characteristic impedance of such a line is 1.18 ohms. In fact, the inter-connecting conductors can be as short as 20 cm to bridge the gap from one condensor terminal to the next, so that real inductance of the high voltage connections can average .2 microhenries per section, producing a time constant of .37 microseconds per section, or a total of 4.5 microseconds for the whole pulse. The characteristic impedance in this case is .535 ohms for a simple type E transmission line. For a Blumlein network using the same capacitors and inductors, the impedance is 1.07 ohms.

The discharge characteristics of the Blumlein under various loads and using various basic assumptions were analyzed computationally using a lumped line Transient Circuit Analysis (TCA) computer program. This program, written in BASIC, has been developed from a previously existing core program. The program is constructed on the nodal circuit analysis principle and is limited only by the capabilities of the computer being used. We have successfully used the program in a 25 element array. Several configuration assumptions were tried starting with the classical "pi" and "T" filter elements and progressing to include the internal inductance of the capacitors and the inductance of the ground line segments between capacitors. We found, in general, that the internal inductance of a capacitor can be lumped with the external inductance with minor effect, so long as the external inductance is several times larger than the internal inductance. The most profound effect of model complexity is in the inclusion of the internal inductance in the model when internal and external inductances are close to the same value. The inclusion of external return-wire inductance is also discernible. This is a peculiarity of our system, since the external inductances are also straight connections between capacitors, and thus, they, the internal inductances and the return lines have similar values of inductances. Only by inclusion of the internal inductance and ground return line inductances were we able to accurately model the currents and voltages at the load and the shorting gap. Figure 4a through 4f show the effects of the changes in mode. Figure 4a shows a conventional model using only external inductance in a 6 element type E lumped transmission line. Figure 4b shows the same as Figure 4a except 20% (.04 microhenries) of the inductance is internal. Figure 4c is the same as Figure 4a except the inductance is partially in the return circuit. Inductance was 0.7 microfareds in all cases. Here we have used only a 6 capacitor array in our model to demonstrate the effects, while limiting computer run time.

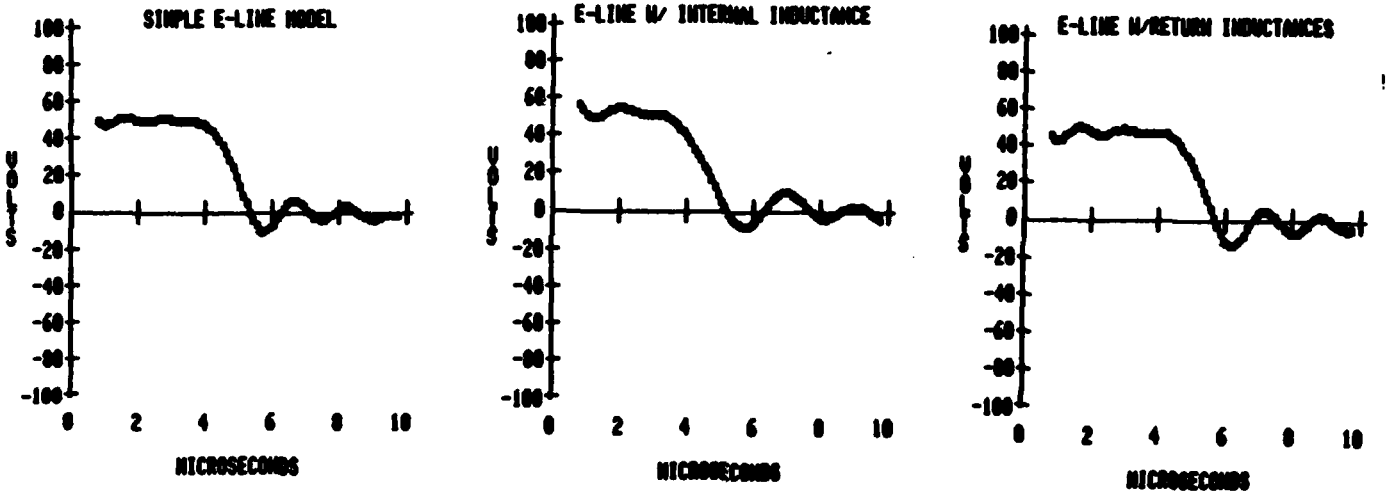

Figure 4. Results of a modelling sensitivity analysis.

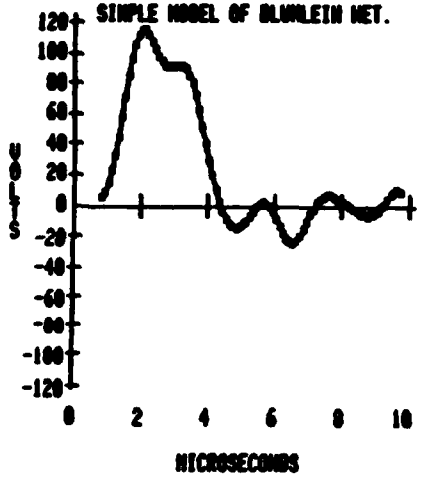

d.

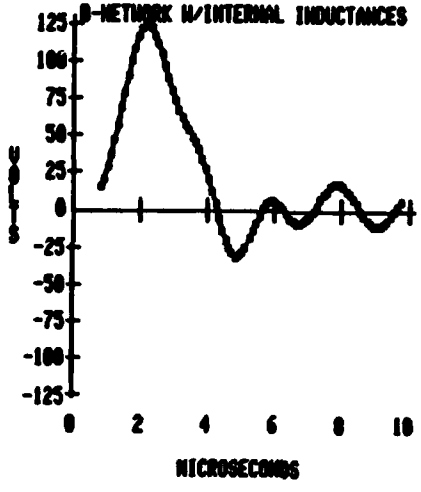

e.

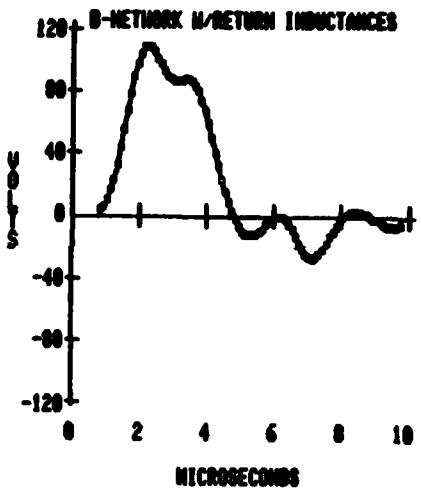

f.

Figure 4. (Concluded)

A short computational analysis was also done to show the effects of unmatched impedances on the response of a Blumlein network which represents, in part, the network which has been built for this project. The hypothesized Blumlein network has only six sections for speed of computation and has the internal inductance included. In the analysis we used six .7 microfarad capacitors which gives half the total capacitance of the experiment. Also, we have adjusted the inductances to produce approximately the same time constant per section for the hypothesized system as we have in the real system. The net result is that each of the external inductors is .16 microhenries and the internal inductance in each capacitor is .04 microhenries except the one which represents the inter-connection between the two sections of the network; it is .9 microhenries. The plasma cell is modelled as a fixed resistor. By computing the system response to various values of the load, we can have a record of the appearance of the responses to compare to those obtained from the experiment. The general discharge characteristics of networks are well documented; nevertheless, the data obtained from this analysis has provided a valuable aid in on-line analysis of the overall system performance.

The characteristic impedance of a perfect Blumlein network using our set-up is:

$$Z = 2 \times (L/C)^{\frac{1}{2}} = 2 \times (.2E\text{-}6/.7E\text{-}6)^{\frac{1}{2}} = 1.07 \text{ ohms} \qquad (2)$$

We have calculated five cases using our short model for various load resistances: (1) R = 10.7 ohms, a very high resistance, ten times Z, (2) R = 2.14 ohms, a resistance twice Z, (3) R = 1.02 ohms, the exact of impedance match case, (4) R = .53 ohms, a resistance one half of Z; and (5) R = 0.107 ohms, a resistance one tenth of Z. Figure 5 is a plot of the peak voltage and fraction of energy in the first pulse vs the normalized load R/2. The five cases are easily distinguished. Figure 6a through 6e show the system responses to these loads. The appearance of the output voltage on a pulse discharged Blumlein network for loads equal to or less than the characteristic impedance. (Note that there are major amplitude changes and wave form changes as the load changes.) Figure 6c shows the exact match case, in which the single triangular pulse carries 94% of the energy to the load and has a peak voltage equal to the charging voltage. The remaining small oscillations eventually carry the remaining energy to the load. Figure 6b shows the same system with a load twice the characteristic impedance, Z. Here, the initial pulse has a peak voltage near one and a half times the charge voltage, and the second pulse is about half the amplitude of the first and has the same polarity as the first. An extreme case of high load resistance is shown in Figure 6a where R = 10.7 ohms = 10 x Z. Here the situation of Figure 6b is exaggerated with the initial pulse being almost twice the charge voltage, and the series of pulses following are gradually declining in amplitude and are the same polarity as the initial pulse. The cases of load impedance lower than Z are shown in Figures 6c and 6d. In Figure 6c the load is one half of Z and the first pulse amplitude is about three fourths of the charge voltage. The second pulse has half the amplitude of the first and is opposite polarity. The succeeding pulses alternate polarity. The case of a very low load resistance is shown in Figure 6d, where R = 0.1-7 ohms = 0.1 x Z. Here, the initial pulse amplitude is low, the second pulse is of opposite polarity to the first, succeeding pulses alternate polarity, and a great deal of "structure" appears in the pulses.

Thus, each category of load resistance is clearly marked by its own peculiarities and is easily distinguished on the trace of a storage oscilloscope.

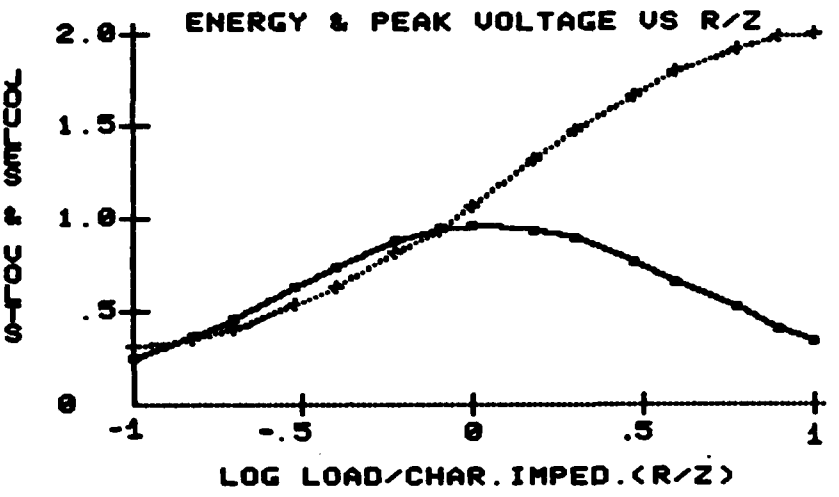

Figure 5. The fraction of total energy in the capacitors in the Blumlein network which is deposited in the load during the first pulse as a function of load ratio, R/Z (solid line) and the peak voltage.

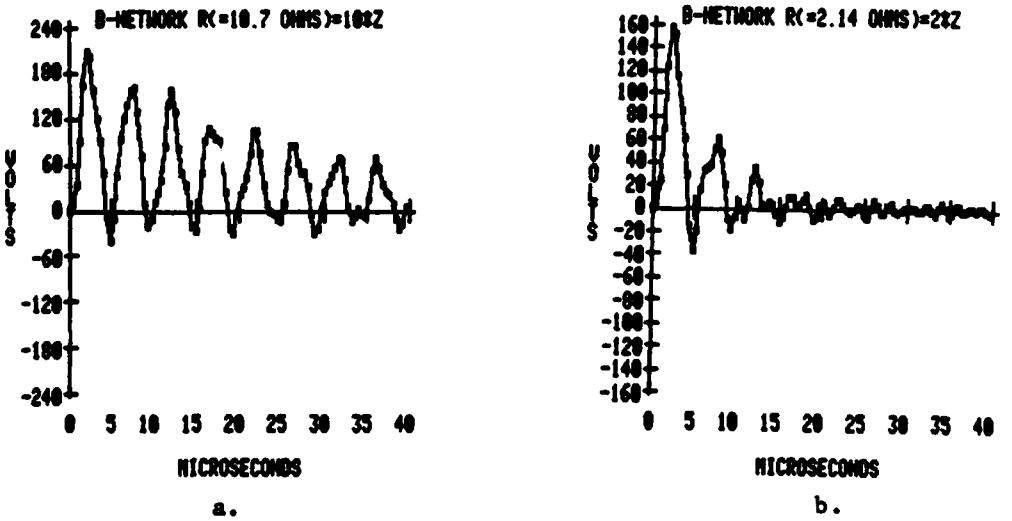

Figure 6. A display of computed voltage wave amplitude and shape on a load 10*Z and 2*Z in a pulsed discharge of a Blumlein network.

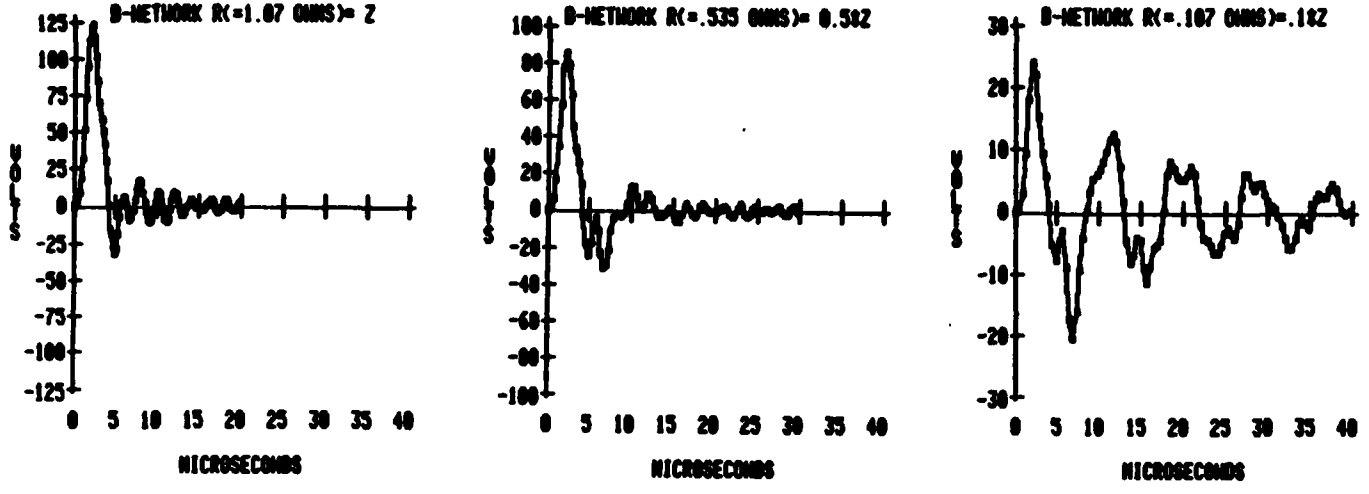

c. d. e.

Figure 6. (Concluded)

The oscilloscope trace of Figure 7 shows a typical response to a load less than Z. Here, it appears that the load is less than one half of Z and greater than one tenth of Z. Other factors complicate the picture for real cases: The inductance and capacitance of the plasma cell change somewhat during the discharge and the resistance of the discharge changes radically during the initial breakdown and in general will continue to decline during the current build-up. A more detailed modelling would include these effects but would require very long computation time, and the results would not reveal additional useful information. The full Blumlein system was modelled from components as shown in Figure 8, and the calculated voltages and currents at the load are shown in Figure 9. Here the load is modelled as an inductance, .18 microhenries, in series with the fixed resistance and this combination is parallel with a 70 picofarad capacitor. This model still could be improved by inclusions of a variable load derived from the measured discharge impedance.

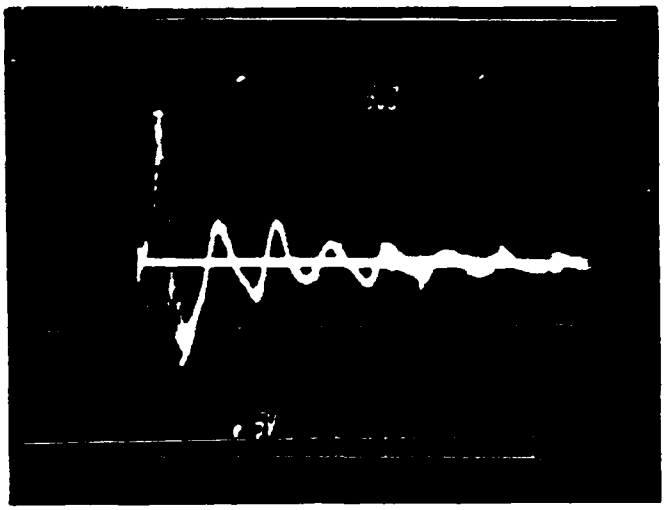

Figure 7. Voltage on the plasma cell with a 300 torr charge of Argon. Note: The Blumlein network was charged to 26 kV. This trace lies somewhere between those of Figure 6d and 6e showing a load impedance in the range of .5Z to .1Z.

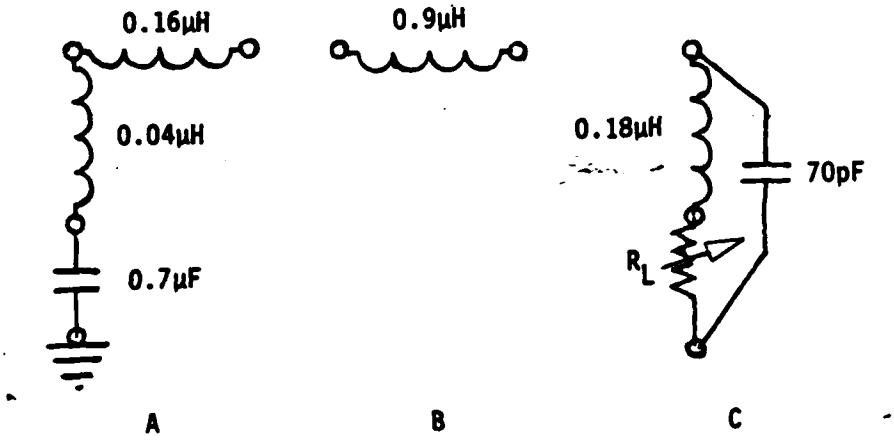

Figure 8. The Blumlein network and load are modelled from the above circuit sub-sets. NOTE: There are 6 each of subset A in each half of the Blumlein network except that the .9μH inductor B, replaces the .16μH inductor in element #6 of the first ~~half~~ of the network. The load, C., is located between the common terminals of the two halves of the network.

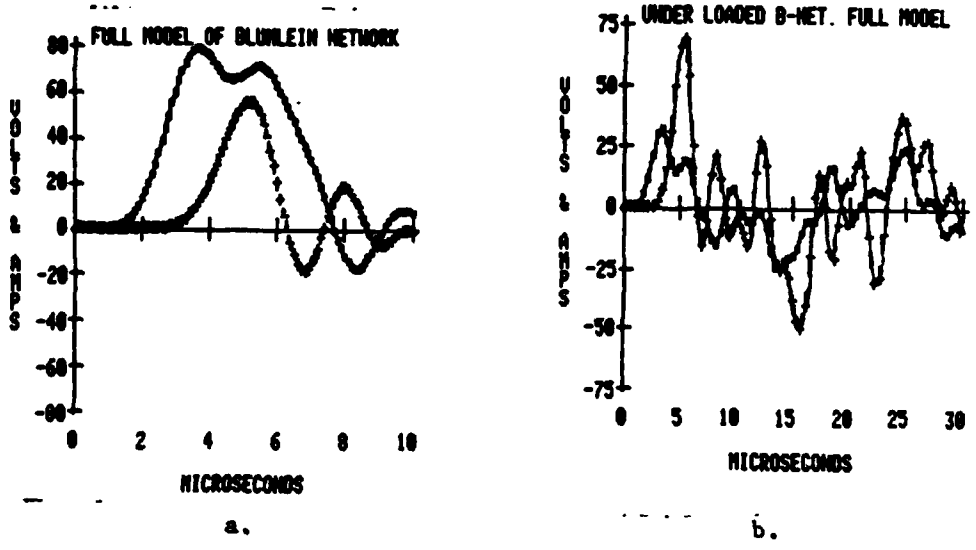

Figure 9. The full model of the Blumlein network with the complex impedance load. NOTE: (a) the "first pulse" for the condition of matched impedance R = Z and (b) for R << Z. The solif lines are current and the broken lines with "+" are voltage. Figure 9.a. would look much like 6c if continued to 30 or 40 microseconds. The phase shift between V and I for the complex reactance can clearly be seen above.

VI. INSTRUMENTATION

In order to properly analyze the operation of the plasma discharge system, it was determined that voltages and currents across the plasma discharge load were desirable, and that some measure of total radiated output, radiative output as a function of time, and some measurement of the spectral distribution of the radiative output as a function of time were necessary.

To measure the output voltage as a function of time a P6015 Tektronix high voltage probe was used. This probe may be fed directly into an oscilloscope - in this case a Tektronix 7834 Storage Oscilloscope - and if adjusted properly has a relatively accurate frequency response. However, this may only be used with the cable length supplied with the probe. Because of the large impedance of the probe, adding additional cable in order to remove the oscilloscope from the electromagnetic radiation generated by the spark gap switch and/or the discharge severely limits the frequency response and consequently distorts the voltage signal significantly. To overcome this, an impedance matching circuit was designed to match the 100 megohm probe impedance to the 50 ohm line. Figure 10 is a schematic of the impedance-matching circuit.

Current was measured by a commercial coil sold by Pearson which is placed around a current-carrying conductor and yields an output of .1 volts per ampere of current across an open circuit. The size coil used was limited to measuring a current of about 5000 amperes. In order to obtain a display of the current of an amplitude amenable to the oscilloscope screen, a 100:1 resistive voltage divider was constructed to attenuate the voltage generated by the current.

The total energy radiated in the spectral band defined by the transmission of Pyrex 7740 glass and the atmosphere was sampled by a Scientech 36-0001 Thermopile head and a 365 Digital readout meter. The transmission of the Pyrex tube, the outer tube of the annular discharge, is shown in Figure 11. The response of the Scientech thermopile as a function of wavelength is flat through the part of the spectrum in which a very large percentage of the radiated energy is located. A molectron joulemeter with a similar flat spectral response was also obtained. It can measure energy in pulses by integration, producing a voltage proportional to the pulse energy. A rather crude estimate of the factor by which the thermopile or joulemeter reading must be multiplied to give the energy radiated by the plasmas through the Pyrex tube for the particular geometry used is 15,000.

Detection devices having EG&G SGD 100A and UV 100 BQ photodiodes were used to obtain the time history of the radiation in the spectral regions where they are sensitive. Spectral response curves of the photodiodes are shown in Figure 12. Total radiation in their acceptance bands was obtained by using the photodiodes unfiltered and without focusing optics which could have affected the spectral band falling on the detectors.

A set of five filters distributed across the visible region of the spectrum was procured in order to obtain the relative radiative intensity in the corresponding portion of the spectrum. These filters pass bands are plotted in Figure 13. In principle, by measuring the radiation in each of

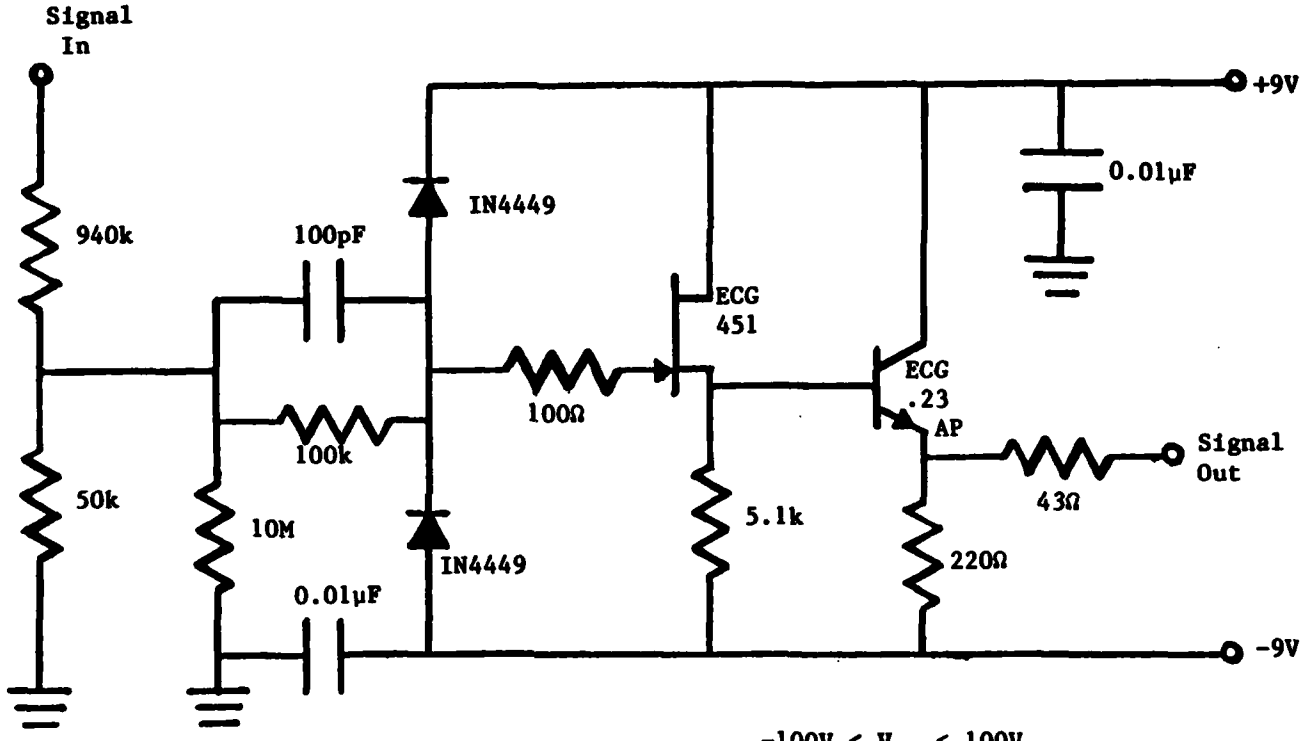

$-100V < V_{IN} < 100V$

$$\frac{V_{OUT}}{V_{IN}} = \frac{1}{40}$$

$R_{IN} = 1\ M\Omega$

$R_{out} = 50\Omega$

Figure 10. Impedance-matching circuit for Tektronix P6015 High Voltage Probe.

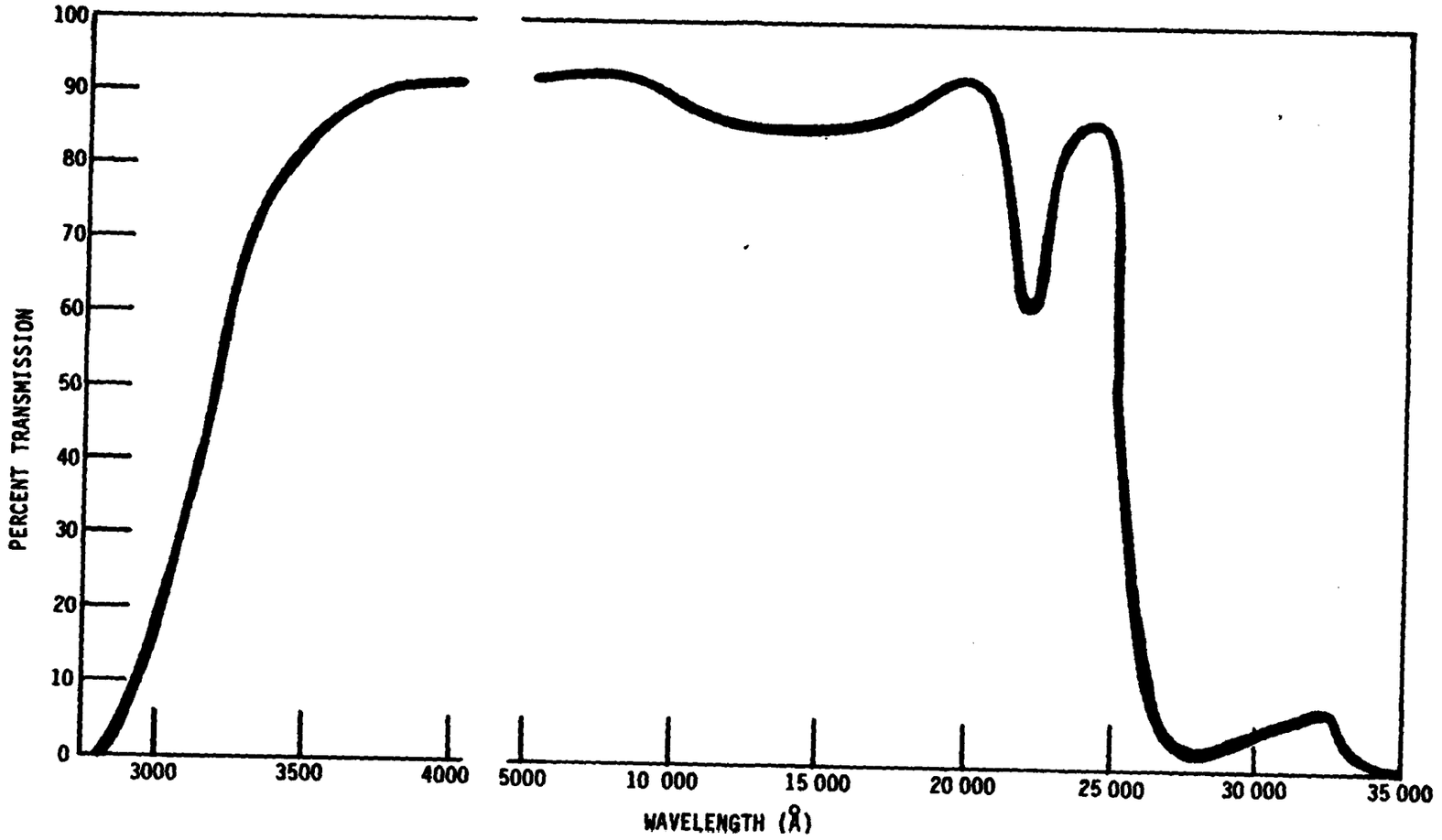

Figure 11. Transmission of Pyrex outer walls vs wavelength.

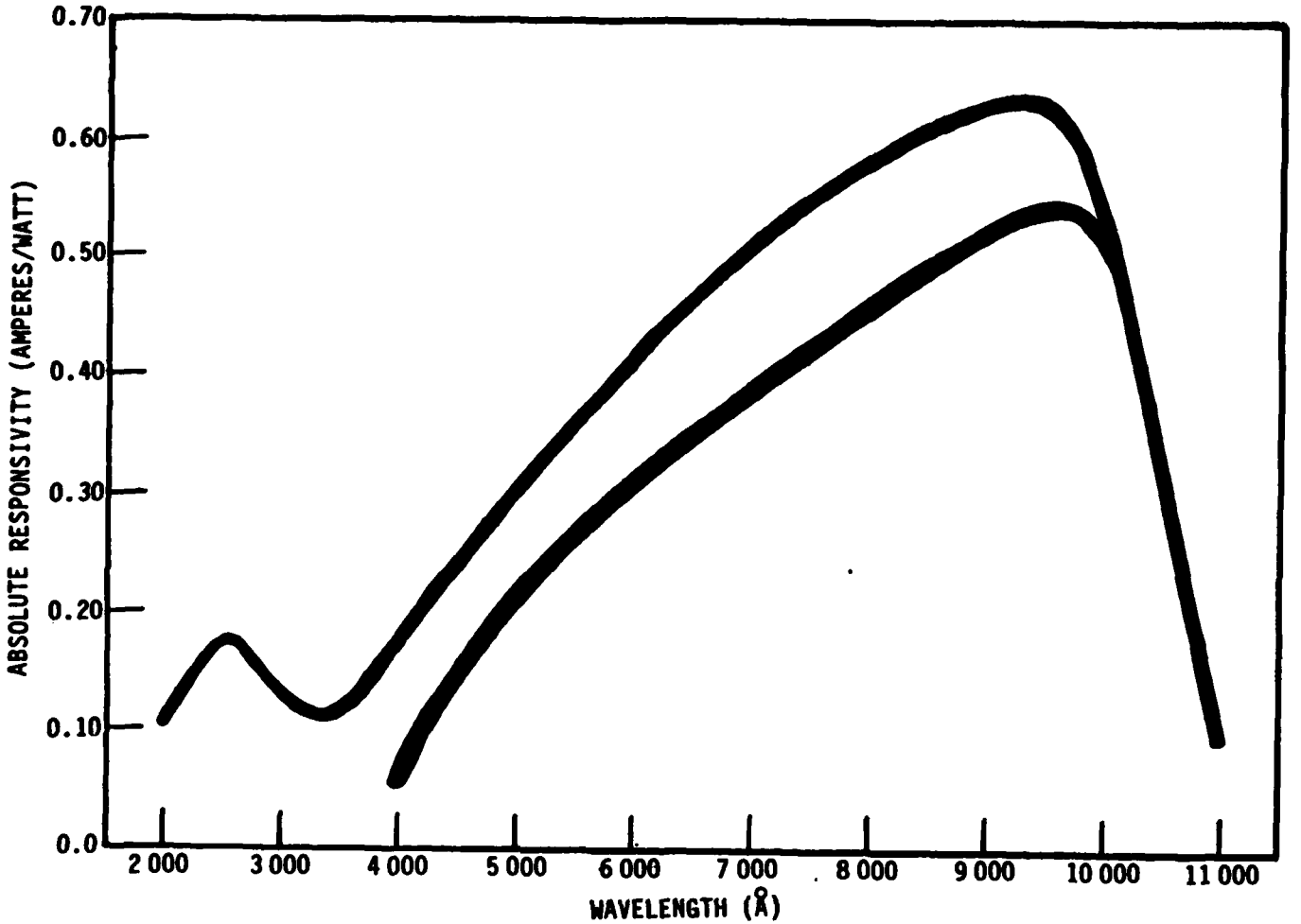

Figure 12. Response of EG & G UV 100 BQ (top) and EG & G 100 A photodiodes as a function of wavelength.

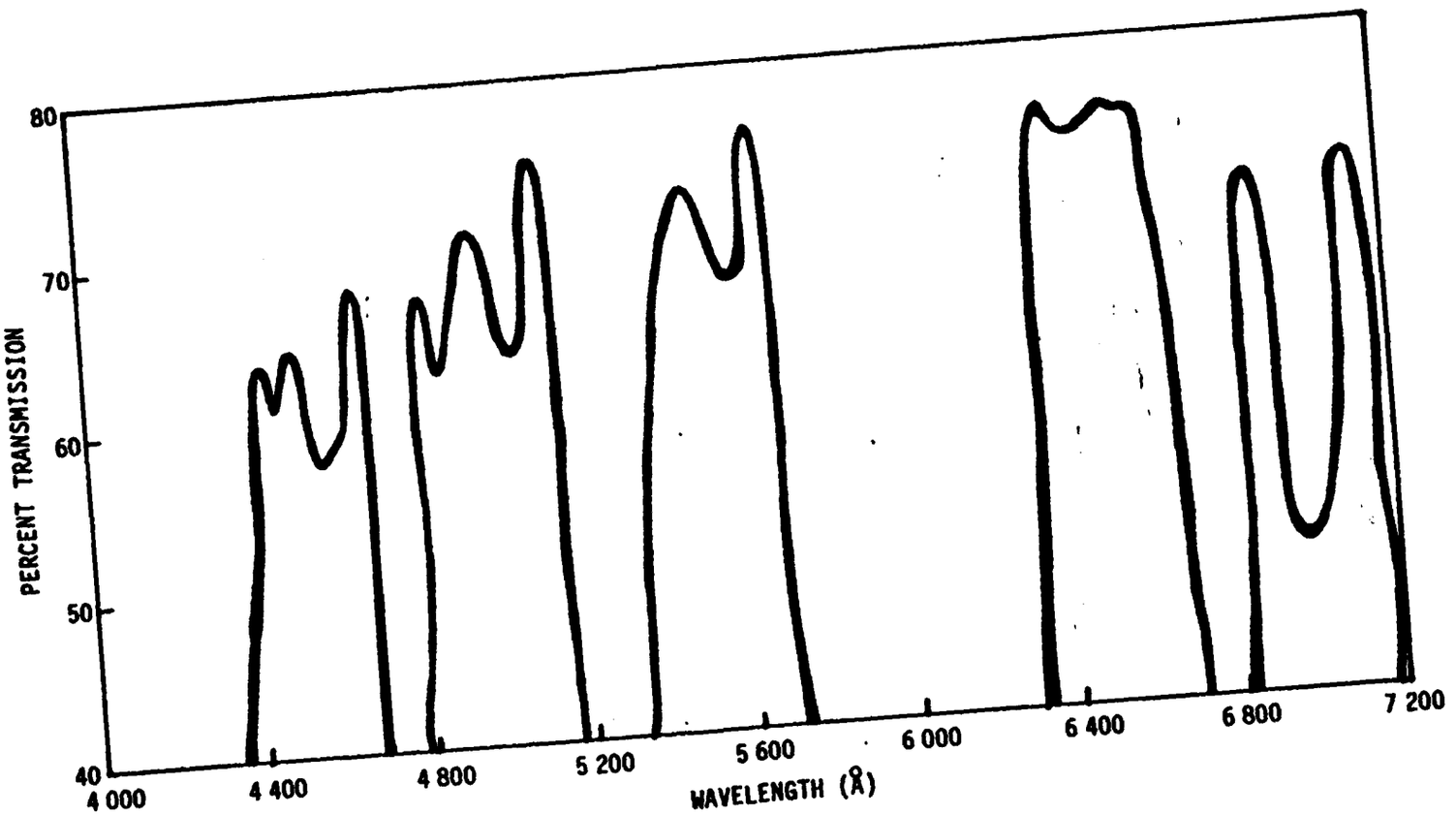

Figure 13. Transmission of set of bandpass filters as a function of wavelength.

these filter pass bands and making corrections for total radiative energy emitted, filter transmission percentage, filter spectral band width, and relative detector response curves, the resulting data may be compared to the ratios of the radiation in the various filter pass bands from blackbody curves of varying temperature, and an equivalent blackbody - or gray body - temperature obtained. The integrity of these results depend, of course, on how closely the radiation of the plasma approximates a blackbody, and how much of the radiative content is spectral line or band radiation.

One of the SGD 100A photodiodes was mounted in an EG+G Lite-Mike having a collecting lens, a bias circuit, and various sensitivity switches having different load resistors for measuring instantaneous power versus time. It also was equipped with a series of integration circuits for measuring energy with various levels of sensitivity. The other photodiodes were mounted in cylindrical holders with provision for removable collecting lenses and filters. A series of filter holders for the bandpass filters was constructed for all the radiation gathering instruments.

For design, checkout, and rough calibration purposes a light chopper was constructed using a 3000 rpm alternating current motor and a chopper disk with 12, .5 inch diameter holes equally spaced around the periphery. The chopper was used to modulate the output from a Dolan-Jenner Model 170-D high intensity light source which has a halogen quartz lamp operated at a color temperature of about 3200°K. This produces a repetitive signal for the detectors which, in all the detectors other than the Scientech thermopile, may be displayed on an oscilloscope.

The signal generated by the chopper was found not to be useful for looking at detection system time constants because of the rather slow pulse rise time involved in the geometry of the light source-chopper arrangement.

In order to provide a signal suitable for observing rise time, a circuit was designed using an operational amplifier to drive a light emitting diode (LED). A schematic of this circuit is shown in Figure 14 and an oscilloscope trace of the pulse form is shown in Figure 15. The device was adjustable in both pulse repetition frequency and light intensity.

Frequency response was observed by displaying the LED driving signal on the oscilloscope along with the detector output. Comparing the shape of the detector output trace with the driving signal gave a measure of frequency response. Adjusting the detector bias voltage and load resistor until the pulse shapes were virtually identical meant that the detector frequency response was adequate for the purpose of this experiment. Although the LED driver pulse was trapezoidal instead of square, the sharp corners at the top of the rise ane beginning of the fall gave a good measure of frequency response. Figure 16 shows oscilloscope traces of a detector signal with and without good frequency response compared to the signal of the driver circuit.

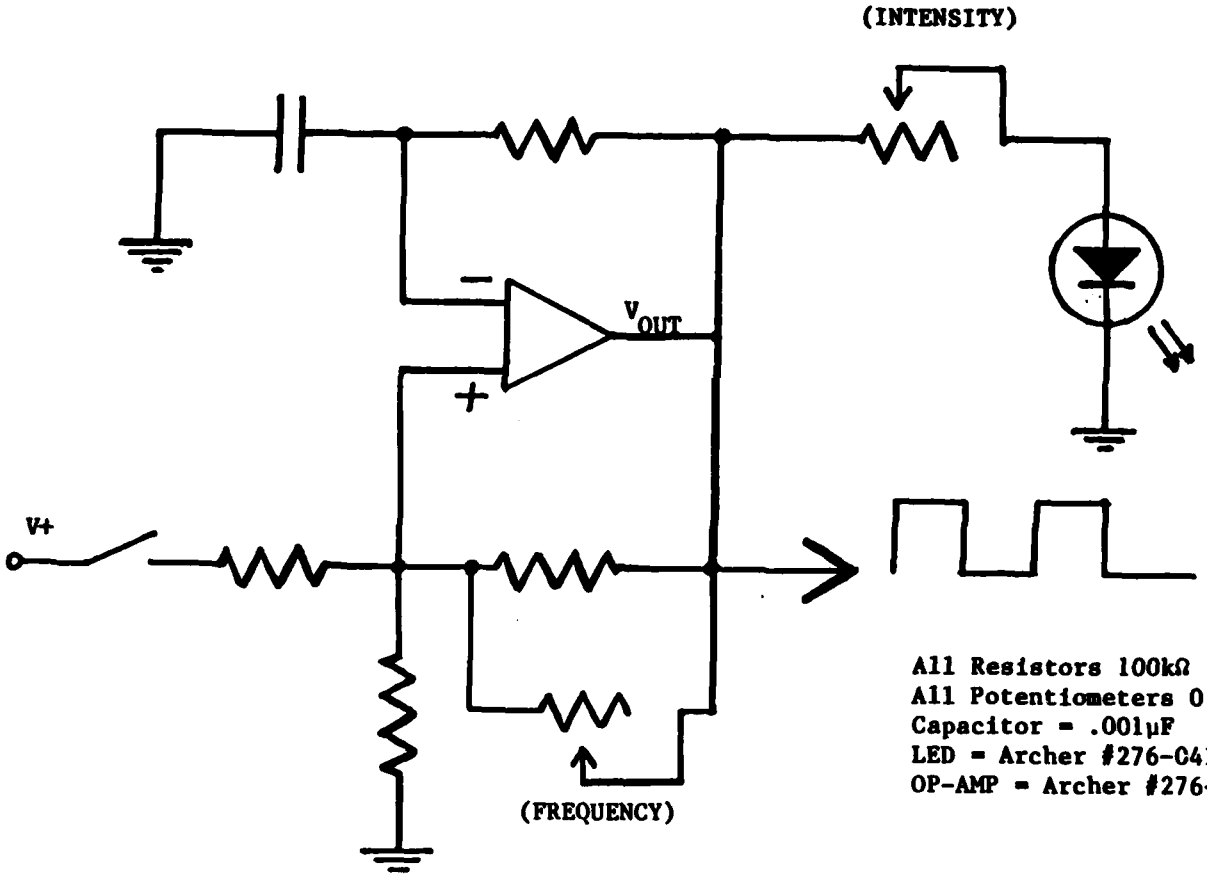

All Resistors 100kΩ
All Potentiometers 0 - 1 Meg ohm
Capacitor = .001μF
LED = Archer #276-041
OP-AMP = Archer #276-1711

Figure 14. Pulsed Light Emitting Diode circuit.

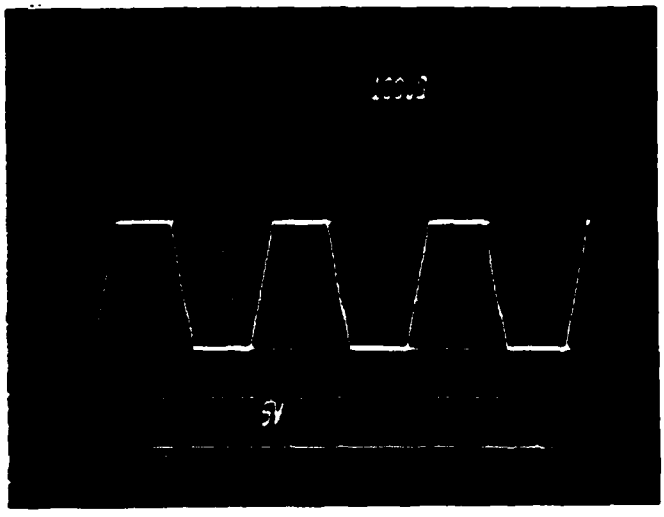

Figure 15. Oscilloscope trace of the Light Emitting Diode driving signal.

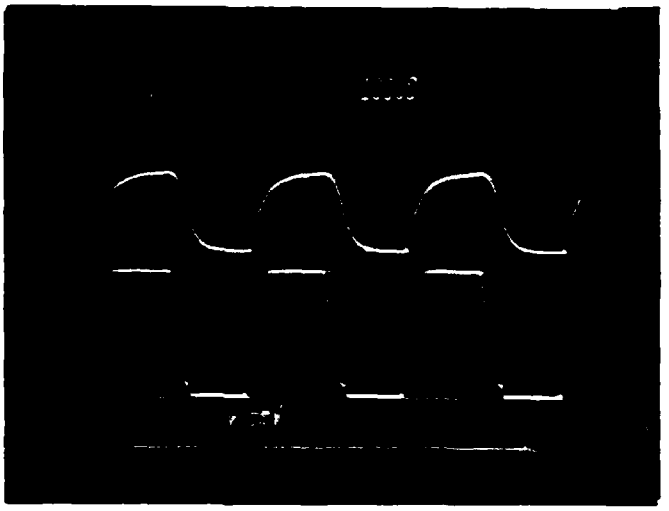

Figure 16a. Oscilloscope trace of Light Emitting Diode driver signal (bottom) and detector output signal (top) with poor frequency response.

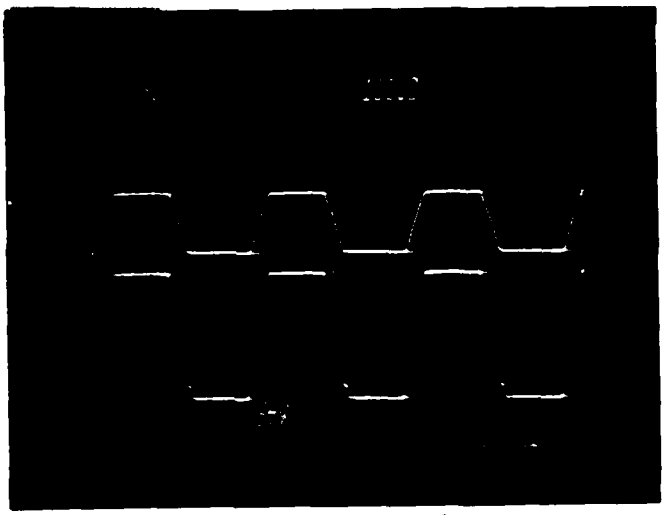

Figure 16b. Oscilloscope trace of Light Emitting Diode driver signal (bottom) and detector output signal (top) with good frequency response.

VII. EXPERIMENTAL RESULTS

A number of firings of the capacitor bank in the Blumlein circuit configuration were conducted for instrumentation checkout purposes. These were at charge voltages ranging from very low - below 1000 volts - to voltages up to about 25 kilovolts. Since the capacitors are rated at 50,000 volts, these higher voltage firings represented stored energies up to 25% of the maximum capability of the bank. Many of these firings were to check out the instrumentation and the shape of the voltage and current pulses. A number of shots were made using a primarily resistive load with as low an inductance as possible. Much of the instrument checkout work was donw with the instruments reading near or directed toward the spark gap. Firing voltages were varied by changing the spark gap spacing. The current measuring loop was placed around one of the mounting posts for the spark gap electrodes, the high voltage probe was placed at one of the gap electrodes and grounded at various points in the circuit, and a detector using one of the photodiodes was directed to the space between the electrodes.

This arrangement allowed for comparison of the light output from the spark with the current and voltage reading. The light output was found to follow the current pulse shape very closely, with due allowance for the fact that the light output is always positive, whereas the current is both positive and negative. Figure 17 is an oscilloscope trace of the light and current outputs at the spark gap.

The set of bandpass filters whose transmission curves are shown in Figure 13 were also used in combination with the photodiode detection system to see if a blackbody temperature for the spark gap could be obtained. The output of the shortest wavelength filter appeared to be anomalously large in these tests, as it may have been in subsequent tests on the plasma tube.

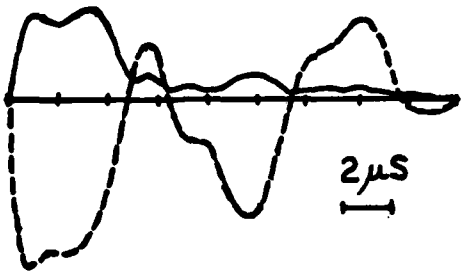

Figure 17. Lite Mike output (solid line) and current coil output (dashed line) as functions of time, taken at the spark gap.

To see if the filter was passing radiation in the infrared, it was used in combination with Schott KG1 and KG3 heat blocking filters. Transmission curves of these filters are depicted in Figure 18. These tests indicated that some infrared was being transmitted through the filter, but only enough to change the reading 6 or 7%, which would not account for the output seen, if the spark gap were a blackbody source. Unless there is significant line radiation in this filter's passband, its larger readings are not yet explained.

When tests were done discharging the bank into the tube containing a gas, the current loop was placed around one of the return rods on the outside of the plasma tube, and a voltage divider was attached across the high voltage input and ground.

Radiation as a function of time from the plasma was observed with a photodiode instrument and the various filters and an integrated energy measurement was made with the Scientech thermopile. The photodiode was used with the filters to try and obtain estimates of color temperature. Figure 19 is a representative oscilloscope trace from the photodiode seen with the blue filter in place. The detection reading on the oscilloscope, observing the plasma tube from the outside, is related to the radiation from the source in the following manner:

$$R_D = R_S(\lambda)\ T_P(\lambda)\ G(A_S,\ A_D,\ f,\ G_S,\ d,\ \theta)\ T_f(\lambda)\ D_R(\lambda,0) \qquad (3)$$

where R_D is reading of the detector, λ is the wavelength of radiation, $R_S(\lambda)$ is the source radiation, and $T_P(\lambda)$ is the transmission of the Pyrex outer tube of the discharge chamber. G is a geometric factor depending on the source size (A_S) and geometry (G_S), the detector area (A_D) and field of view (f), and the distance (d) and angle (θ) from the source to the detector; T_f is the filter transmission and D_R is the detector response, a function of the wavelength and detector optical system (0). In measurements to obtain a color temperature, the geometry factor was held constant and the transmission of the discharge outer wall was considered a constant. The detector outputs were corrected for the filter transmission and detector response, and the reading of the total energy from the thermopile was used to normalize for shot-to-shot variation, as long as the variation was small enough not to seriously affect the color temperature.

The energy measurement from the Scientech thermopile was not corrected for detector response, as it is flat through the region of the spectrum being observed. There were no optics in the system and the filters were not used, so only the geometric factors were involved. These were held constant throughout the experiments and, as mentioned earlier, a single number representing the geometric factor was used to estimate total radiant energy transmitted through the Pyrex outer wall. The fraction of the total energy that is transmitted through the Pyrex is dependent on the temperature for blackbody radiation, dropping sharply as the color temperature increases to high levels. These ratios have been computed for the range of 5000°K to 50,000°K and are listed in Table 3. This table is derived from a calculation of the ratio of

$$\frac{\int_{\lambda_1}^{\lambda_2} T_p(\lambda)\, d\lambda}{\sigma T^4} \qquad (4)$$

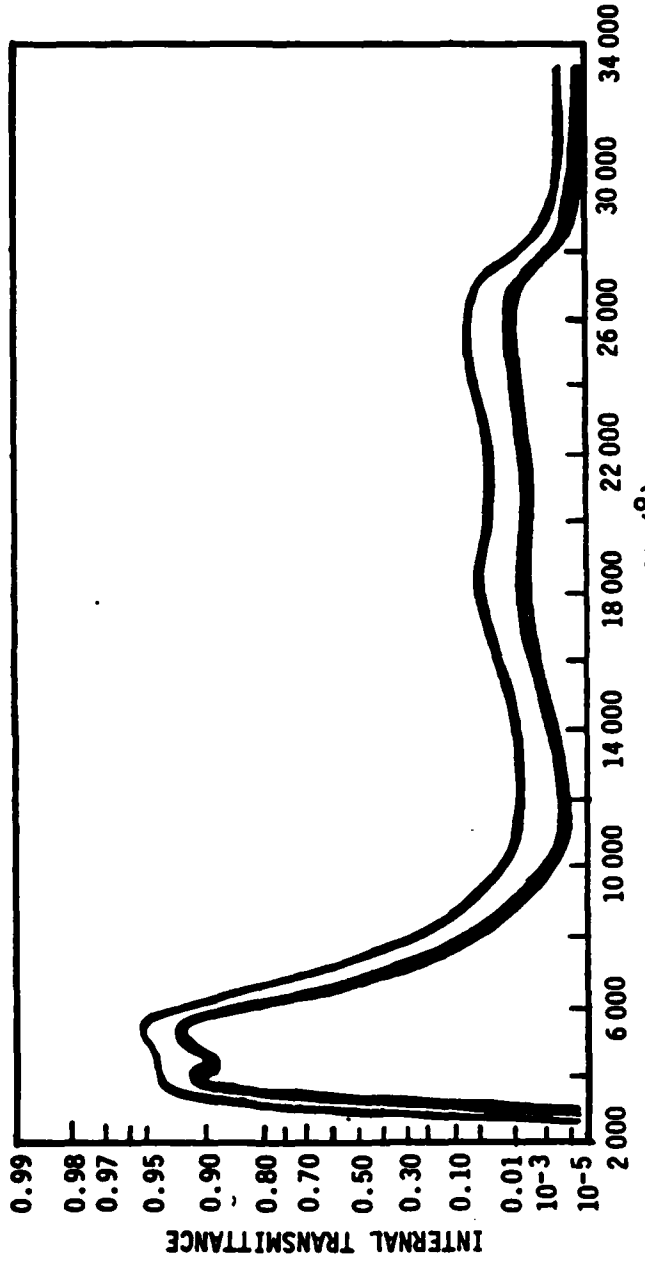

Figure 18. Transmission as a function of wavelength for Schott KG 1 (top) and KG 3 (bottom) heat blocking filters.

where λ_1 and λ_2 are the short and long wavelength cutoff frequencies of the Pyrex tube, σ is the Stefan-Boltzmann constant ($=.567 \times 10^{-11}$ joules sec^{-1} cm^{-2} $°K^{-4}$), and T is the temperature in °K.

TABLE 3. Fraction of Blackbody Radiation Transmitted by Pyrex at Various Temperatures.

Temp (°K)	Radiation (watts/cm^2	Fraction transmitted by Pyrex
5000	3.6×10^3	.72
10000	5.7×10^4	.48
20000	9.2×10^5	.15
30000	4.6×10^6	.06
40000	1.4×10^7	.03
50000	3.4×10^7	.02

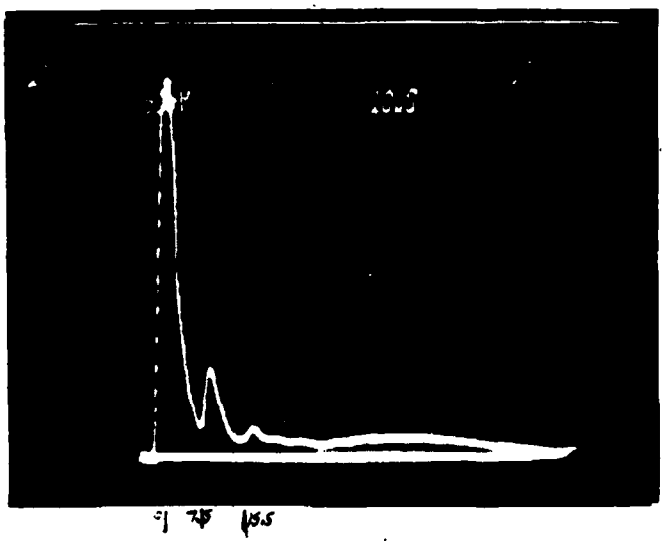

Figure 19. Photodiode output vs time with blue filter in place. Radiation from plasma cell filled with 50 torr argon.

A series of shots were made at fill pressure of 100 torr and 300 torr argon. Tables 4 and 5 list readings of total energy based on the Scientech thermopile, along with the firing voltage estimated from the current and voltage readings on the power supply.

TABLE 4. Plasma Radiation Energy from 100 Torr Argon Transmitted Through Pyrex From Thermopile Total Energy Measurements.

Firing Voltage (kilovolts)	Thermopile Reading (joules x 10^3)	Estimated Source Energy Transmitted (joules)
15.3	1.07	16
15.5	1.10	16
15.7	1.12	17
15.2	1.03	15
14.7	1.00	15
15.5	1.06	16
14.5	.89	13
14.6	.87	13

TABLE 5. Plasma Radiation Energy From 300 Torr Argon Transmitted Through Pyrex From Thermopile Total Energy Measurements.

Firing Voltage (kilovolts)	Thermopile Reading (joules x 10^3)	Estimated Source Energy Transmitted (joules)
21.5	2.60	39
18.6	1.91	29
19.0	1.97	30
18.1	1.77	27
17.9	1.68	25
20.7	2.17	33
18.9	1.93	29

To obtain the total energy radiated by the plasma, it is necessary to multiply these transmitted energy values by the inverse of the proper ratios listed in Table 3 for the plasma color temperature. As may be noted from this table, this factor may be as large as 50 for a temperature of 50,000°K.

The relationship of the Pyrex transmission band to the blackbody curve is illustrated for two temperatures in Figure 20.

Data were taken using the photodiode detector with the filter set for plasma tube fillings of 50, 100, and 300 torr argon. Firing voltage and total energy readings were approximately the same for the 50 and 100 torr runs, but the voltage was higher and the energy about twice as much for the 300 torr shots. The raw readings were reduced as described above and are plotted in Figure 21. Attempts were made to fit these points to various blackbody temperature curves without complete success. However, assuming a blackbody distribution, it may be inferred from the trend of the data that the peak of the curve is at a wavelength shorter than that in the pass band of the blue filter, indicated a temperature of >7000°K, and perhaps much higher than 10,000°K. To obtain this temperature more accurately by this method requires additional filters at shorter wavelengths.

VIII. LIGHT EMISSION AS RELATED TO PLASMA PROPERTIES

The light emission has been described in the section on experimental results. We will now attempt to relate the emission of the fastest of the bands, the blue band, to the plasma properties, both electrical and hydrodynamic. Figure 22 is a photograph of the scope trace for the plasma cell for voltage and temporal light response. The light emission starts after the first pulse of energy (∿50%) has been absorbed in the plasma, three microseconds after the start of discharge. The light output timing and pulse shape indicate that it is <u>not</u> coupled directly to the power input. This contrasts markedly from the similar measurements of the light output at the spark gap on the Blumlein network which exactly follows the current pulse in time and amplitude. Figure 17 shows the Lite Mike output and voltage output as functions of time. This may be compared to the current and light output shown in Figure 22 for the plasma cell. We use this lack of correlation to support our hypothesis that the light seen by the Lite Mike plus the blue filter is not directly generated by the electric discharge.

The second possible source of the radiation is the plasma shock wave generated by the collapse of the discharge onto the intermediate tube in the plasma cell. For the plasma, which is generated in the current sheath on the inside of the outer wall of the plasma cell, to collapse the magnetic pressure of the current must exceed the combined gas and plasma pressure inside the sheath. The relation is shown in Equation 5 below:

$$P(\text{gas}) + P(\text{plasma}) > I^2/2\pi r^2 \qquad (5)$$

The best way to follow this type of action is to use a streak camera and watch the plasma sheath move in towards the intermediate tube and then radiate during the collision processes (Reference 4). This action would produce one high intensity pulse. In fact, we see one such pulse followed by

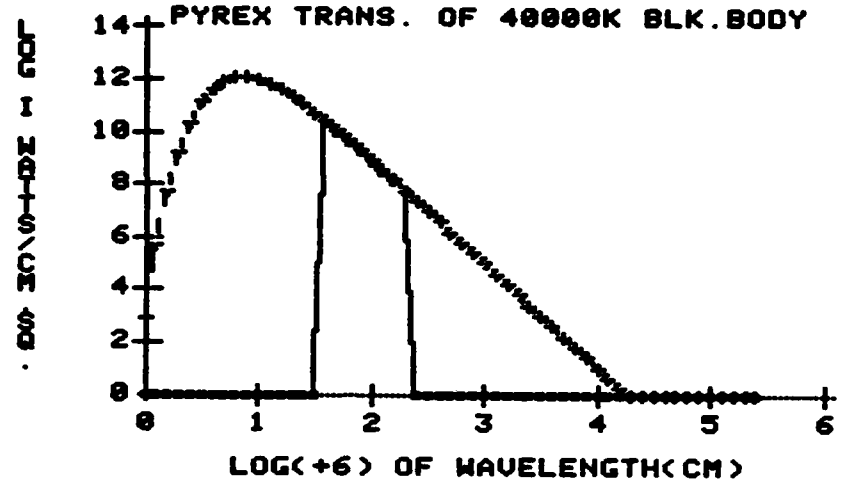

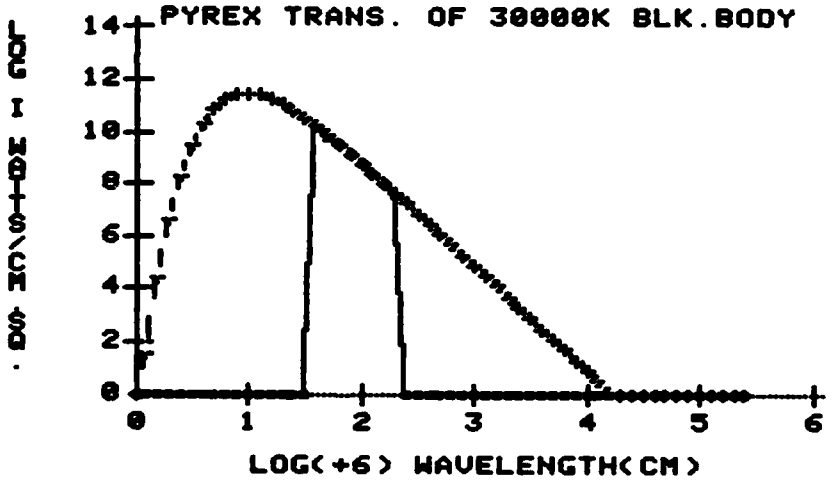

Figure 20. Pyrex transmission superimposed on blackbody curves for temperatures of 40,000°K and 30,000°K. The graph is a plot of the log of intensity in watts/cm^2 vs log plus six of the wavelength in cm.

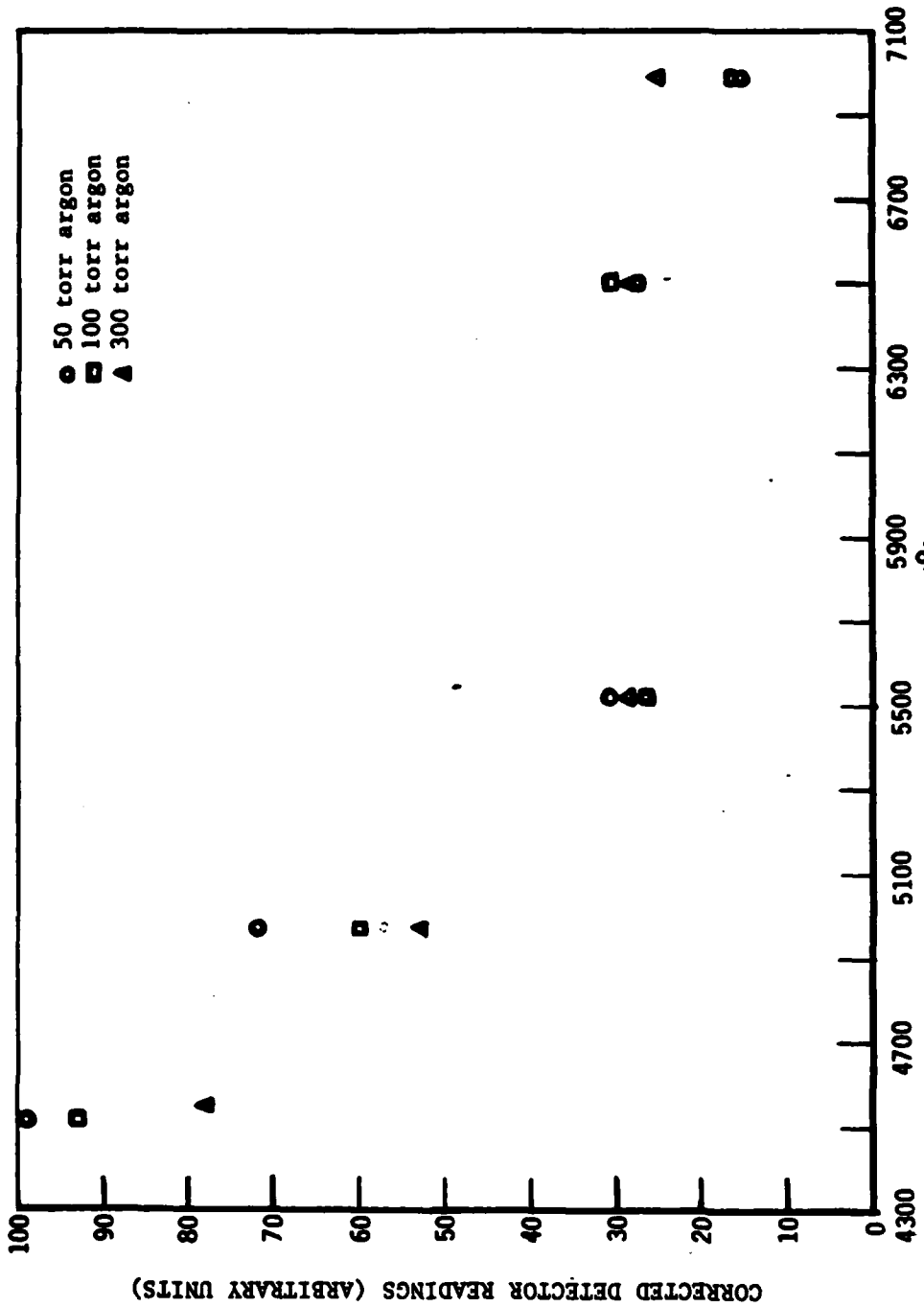

Figure 21. Corrected detector amplitude readings for the set of bandpass filters plotted at bandpass center wavelengths.

one or two smaller pulses at approximately equal intervals. This can easily be seen in Figure 22. The timing of these pulses is such that they could be secondary shock waves arriving at the intermediate tube surface. The time interval, as measured from Figure 22 and other similar data, is 4 microseconds for the main pulse and 12 microseconds for the secondary pulse, as measured from the time of the voltage peak. The gap between the inside of the outer tube and the outside of the intermediate tube is 2.7 cm. Assume that the plasma is formed and starts moving as a shock wave during the time between the start and peak of the current, then "coasts" in as a fully developed shock wave and emits light as the shock energy is converted to heat during collision with the outer wall of intermediate tube. In such a case, the time between the peak of the first current pulse and the peak of the light pulse may approximate the transmit time for the shock wave. We have from the data of Figure 22, a time of 4 microseconds and a velocity of $6x8 \times 10^5$ cm/sec. By using the time interval between the major and first minor light pulse as an indication of the time for the wave to move from the intermediate wall to the other and back again, we have a time of 12 microseconds and a velocity exactly the same as above for the secondary shocks. We do not have suitable instrumentation to analyze the shock structure in the plasma cell, however, the numbers we show above are plausible and the apparent lack of coupling between the radiation output and the electrical input lend support to this analysis.

The above description deviates from the process we had hoped to get, which was simple ohmic heating of a plasma to a temperature between 2 eV and 5 eV. This may still occur since we have only been able to get reliable discharges at 350 torr and lower. Our goal is to get either an all metal plasma or a metal plasma starting a high pressure gas plasma (>1 atmos of argon or krypton). In such a case, there will be considerably more electronic-level radiators than we have now.

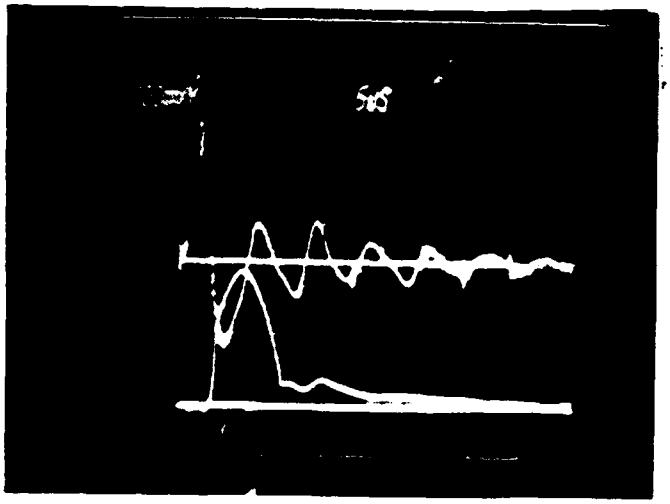

Figure 22. The voltage on the plasma cell (top trace) and the output of the Lite Mike with blue filter (bottom trace) for a 300 torr argon discharge. The main light pulse falls 4 microseconds after the first voltage pulse and the secondary pulse is 8 microseconds later.

IX. POTENTIAL APPLICATIONS EVALUATION STATUS

Potential applications for the laser light source under investigation can only be conjecture at this time. It is expected that the light source can eventually be made to equal the standard xenon lamp in efficiency. The plasma light source, however, will have a pulse length of about ten microseconds compared to several hundred microseconds for the xenon lamp and will have a correspondingly higher intensity up to 100X more intense than the xenon lamp. With these properties, the plasma light source can be used as a fast pump for a Nd:glass laser or for a dye laser or perhaps for a whole new class of lasers which have high pumping thresholds. There is also the possibility that the plasma light source, itself, can be a laser, as we mentioned in our proposal for this work. The experiment equipment is designed for laboratory use only. A complete "fieldable" system would be much more compact. Note that the common plastic-oil dielectrics have a dielectric constant(ϵ) of about 4 where a glycerol has $\epsilon = 44$, water has $\epsilon = 80$, and barium titanate has $\epsilon > 1000$. Thus, depending on the properties, the capacitors may be 5 to 500 times physically smaller than they are now for the same total energy.

Additional information, particularly a good proof-of-principle demonstration experiment, is required before a proper critique of the plasma light source can be made.

X. RECOMMENDATIONS FOR FUTURE DEVELOPMENT

We recommend the continuation of research in the use of the plasma light source to pump Nd:glass and dye lasers. Work in this area will fully exploit the presently available power supply and discharge system installed at The University of Alabama in Huntsville. Variations of parameters experiments should be made to determine the optimum pumping rate on a Nd:glass laser and on dye lasers containing #R6G, #C102, and #S3 dyes. This selection of dyes represents color bands all the way from the yellow to the near ultraviolet wavelengths. Pumping is expected to be vigorous enough to deplete the dyes and the objective is to produce the most dye laser output power that we can.

It should be determined whether or not the plasma can be made to act as a laser. This will require some modification of the present discharge system. An MHD plasma drive discharge apparatus may be the best configuration for this experiment. A collapsing plasma configuration will be used and the shock wave generated by the collapse will heat the plasma and the rarefaction wave following it will cool the plasma with, we expect, the proper inversion to produce laser action.

REFERENCES

1. Turchi, P. J., and Baker, W. L., J.A.P. (USA) 44, 11, pp 4936 (1973).

2. Degnan, J. H., Reinovsky, R. E., Bengston, R. D., and Honea, D. L., J.A.P. (USA), 52, 11, pp 6550 (1981).

3. Baker, W. L., Clark, M. C., Degnan, J. H., Kiuttu, G. F., McClenaham, C. R., and Reinovsky, R. E., J.A.P. (USA), 49, 9, pp 4694 (1978).

4. Roberts, T. G., "Experimental Verification of Self-Focusing in Intense, Relativistic, Electron Beams", Ph.D. Thesis, North Carolina State University, Raleigh, NC (1967).

5. Benjamin, R. F., Pearlman, J. S., Chu, E. Y., and Riordan, J. C., App. Phys. Lett. 39, 10, 00 848 (1981).

6. Gersten, M., Rauch, J. E., Clark, W., Richardson, R. D., and Wilkinson, G. J., App. Phys. Lett., 39, 2, pp 148 (1981).

7. Hussey, T. W., Roderick, N. F., and Kloc, D. A., J.A.P. (USA), 51, 3, pp 152 (1980).

8. Lee, Ja. H., McFarland, D. R., and Hohl, F., Appl. Opt., 19, 19, 00 3343 (1980).

9. Fanning, J. F., and Kim, K., "A Mather-Type Dense Plasma Focus as a New Optical Pump for Short Wavelength High Power Lasers," Paper WWS, CLEO'83, Baltimore, MD (1983).

10. Gilder, Jules H., Basic Computer Programs in Science and Engineering, Hayden Book Co., Rochelle Park, NJ (1947).

11. Grover, Fredrick W., Inductance Calculations: Working Formulae and Tables, Instrument Society of America, Research Triangle Park, NC (1982 reprint).

12. Snow, Chester, "Formulas for Computing Capacitance and Inductance," NBS Circular #544, U.S. Gov't Printing Office, Washington, DC (Sept. 10, 1954).

13. Englehardt, A. G., and Phelps, A. V., "Elastic and Inelastic Collision Cross Section in Hydrogen and Deuterium from Transport Coefficients," Physical Review, V. 131, No. 5, pp 2115-2128, 1 Sept 1963.

14. Taylor, R. L., Caledonia, G., Lewis, P., Wu, P., Tear, J. D., and Cronin, J., Analytical Modeling of Electrically Excited D2/HCl and HCl Laser Experiments, PSI TR-58, Final Report, Physical Sciences Laboratory, Woburn, Mass, (July 1976) sponsored by Office of Naval Research, Arlington, VA 22217 (Gov't Acc. No. DN 480-222).

DISTRIBUTION

	No. of Copies
Director US Army Systems Analysis Activity ATTN: DRXSY-MP Aberdeen Proving Ground, MD 21005	1
Central Intelligence Agency ATTN: OIA/TSO, Mr. L. Echenrode OSWR/DSD, Mr. G. Bock Washington, DC 20505	1 1
DOD Nuclear Effects Information and Analysis Center (DASIAC) Defense Technology Information Repository (DETIR) Kaman Tempo ATTN: Mr. F. Wimenitz 2560 Huntington Ave Alexandria, VA 22303	1
DASIAC-DETIR Kaman Tempo ATTN: D. Reitz 816 State Street (P.O. Drawer QQ) Santa Barbara, CA 93102	1
Army Library ATTN: ANR-AL-RS (Army Studies) Pentagon, Washington, DC 20310	1
Department of Physics, UAH ATTN: Dr. Barr Dr. McKnight Huntsville, AL 35899	1 1
BMDATC-R, Dr. Dezenberg	1
BMDATC-E, Dr. Jones	1
AMSMI-R, Dr. McCorkle Dr. Rhoades	1 1
AMSMI-RPR	15
AMSMI-RH	1
AMSMI-RHS, Dr. Honeycutt	1
AMSMI-RHS, Mr. Ehrlich	1
AMSMI-RHC, Mr. Cole	2
AMSMI-RPT (Record Set)	1

DISTRIBUTION (Concluded)

	No. of Copies
IIT Research Institute ATTN: GACIAC 10 W 35th St Chicago, IL 60616	1

END

FILMED

11-85

DTIC